Eoarchaean tectonics

Hastie, Alan; Fitton, Godfrey

DOI:
10.1016/j.precamres.2019.02.006

Document Version
Peer reviewed version

Citation for published version (Harvard):
Hastie, A & Fitton, G 2019, 'Eoarchaean tectonics: new constraints from high pressure-temperature experiments and mass balance modelling', *Precambrian Research*, vol. 325, pp. 20-38.
https://doi.org/10.1016/j.precamres.2019.02.006

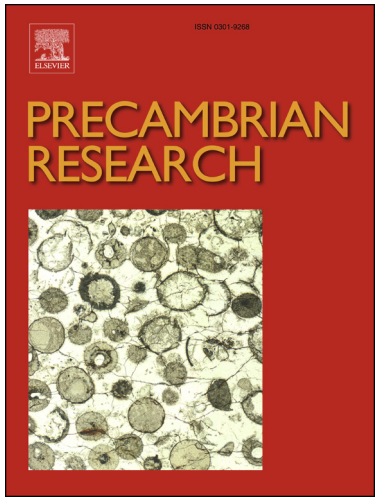

Eoarchaean Tectonics: New constraints from high pressure-temperature experiments and mass balance modelling

Alan R. Hastie, J. Godfrey Fitton

PII: S0301-9268(18)30491-1
DOI: https://doi.org/10.1016/j.precamres.2019.02.006
Reference: PRECAM 5281

To appear in: *Precambrian Research*

Received Date: 21 September 2018
Revised Date: 1 February 2019
Accepted Date: 12 February 2019

Please cite this article as: A.R. Hastie, J. Godfrey Fitton, Eoarchaean Tectonics: New constraints from high pressure-temperature experiments and mass balance modelling, *Precambrian Research* (2019), doi: https://doi.org/10.1016/j.precamres.2019.02.006

Eoarchaean Tectonics: New constraints from high pressure-temperature experiments and mass balance modelling

Alan R. Hastie[a] and J. Godfrey Fitton[b]

[a] *School of Geography, Earth and Environmental Sciences, University of Birmingham, Edgbaston, Birmingham B15 2TT, U.K.*
[b] *School of GeoSciences, University of Edinburgh, King's Buildings, Edinburgh, EH9 3FE, U.K.*

*Corresponding author: E-mail: a.r.hastie@bham.ac.uk. Present address: School of Geography, Earth and Environmental Sciences, University of Birmingham, Edgbaston, Birmingham B15 2TT

E-mail addresses: a.r.hastie@bham.ac.uk (A.R. Hastie) and godfrey.fitton@ed.ac.uk (J.G. Fitton)

Abstract

Four billion years ago the formation and preservation of the Earth's first continental crust marked a new stage in the long-term geochemical evolution of our planet. This continental material is predominantly composed of plagioclase-rich granitoids that form Eoarchaean Tonalite and Trondjhemite (ETT) rock suites. There are two plausible overarching models for generating ETT: by a variety of intraplate melting mechanisms or through the onset of primitive subduction. Here we use mass balance modelling to show that ETT can only be derived from the hydrous melting of mafic rocks in convergent margins. These mafic source regions could be composed of relatively undepleted (oceanic plateau-like) non-arc metabasalts with or without residual rutile. Melts derived from these metabasalts subsequently mix with a slab-related component to form ETT magmas. Additionally, ETT can be formed from partial melting of metabasalts with geochemical affinities similar to modern island arc basalts. We propose that a primitive form of plate tectonics began on the surface of Hadean magma ocean(s), in a similar way to the plate-like motions observed on modern lava lakes, and subsequently evolved into the plate tectonics operating today. Hydrous melting of subducted basaltic crust and the formation of the proto-continental ETT crust would have followed the onset of accumulation of liquid water on the Earth's surface.

Keywords: Eoarchaean Earth, Tonalite, Trondhjemite, Granodiorite (TTG), Mass balance modelling, Slab flux, Rutile, Subduction, Plate tectonics.

1. Introduction

The presence of both oceanic and continental crust, large volumes of liquid water and active plate tectonics are three interlinked fundamental characteristics that distinguish the modern Earth from other planets in our solar system. Nonetheless, we still cannot agree when these three characteristics developed. How the continents initially formed and when plate tectonic-like processes developed is important because both are ultimately responsible for modifying the composition of Earth's early geochemical reservoirs, which have subsequently evolved into the present-day mantle, hydrosphere and atmosphere.

Zircons from the Jacks Hills conglomerates, Australia suggest that continental crust existed ~4.4 Ga (e.g., Harrison et al., 2005; Hopkins et al. 2008). These early ages, however, are obtained on detrital zircons from much younger rocks, whose protolith has long since been destroyed or reworked (O'Neil et al., 2007). The oldest stable and *preserved* juvenile continental crust began forming on the Earth, and possibly on other terrestrial planetary bodies (Sautter et al. 2015), ~4 billion years ago (e.g., Bowring and Williams, 1999; Nutman et al. 1999; 2009, Hoffmann et al. 2011). These ancient rocks are found in West Greenland (Baadsgaard et al., 1986, Crowley, 2003, Nutman and Friend 2009), Australia (Nutman et al., 1993, Kinny and Nutman, 1996), Antarctica (Harley and Black 1997), China (Liu et al., 2007, Ge et al., 2018) and Canada (Bowring and Williams, 1999, Iizuka et al., 2007, O'Neill et al., 2007). Nevertheless, the tectonic processes responsible for generating this ancient continental material are poorly understood and rival hypotheses of a dominant horizontal vs. vertical geodynamic regime are still hotly debated (Ernst et al. 2016; Hawkesworth et al., 2016, 2017, Hastie et al., 2016a, Kaczmarek et al., 2016, Rozel et al. 2017, Cox et al. 2018, Ge et al., 2018, Keller and Schoene 2018, Moyen and Laurent 2018, Wiemer et al., 2018). Accordingly, the timing of the initiation of plate tectonics resembling either modern subduction zone processes or atypical subduction, is also highly contentious with estimates ranging from <1.0 to >4.0 Ga (Harrison et al. 2005; Jenner et al. 2009, Nutman et al. 2009, Dhuime et al. 2012, Foley et al., 2014; Nebel et al. 2014, Hastie et al. 2016a, Hawkesworth et al. 2016, Stern et al. 2016; Keller and Schoene 2018, Ge et al. 2018).

Although Archaean time scales are debated (Kamber 2015), the oldest part is generally considered to be represented by the Eoarchaean Era from 4.0-3.6 Ga. No continental rocks (sensu stricto) from before the Eoarchaean, or the Eoarchaean/Hadean boundary, have yet been discovered and up to 90% of the earliest surviving continental crust from ~4.0-3.6 Ga is composed of plagioclase-rich granitoids that form Eoarchaean Tonalite and Trondjhemite (ETT) rock suites (Baadsgaard et al., 1986, Bowring and Williams, 1999; Nutman et al. 1999; 2009, Crowley, 2003, Steenfelt et al., 2005, Iizuka et al., 2007; Liu et al., 2007, O'Neil et al., 2007; Hoffmann et al. 2011, Polat et al., 2015). Granodiorites (G) are commonly included as an ETT(G) suite but the granodiorites, and potassic granites, are generally younger and are interpreted as being derived from melting older ETT (Baadsgaard et al., 1986; Numan et al., 1993; Kinny and Nutman, 1996; Crowley, 2003; Steenfelt et al., 2005; Nutman et al. 2007; 2009; Nutman and Friend 2009; Polat et al., 2015; Hoffmann et al., 2014). Nevertheless, exceptions do exist: see Bowring and Williams, 1999 and Iizuka et al., 2007 for examples of ~4.0 Ga granodiorite and granite from the Acasta Gneiss Complex respectively. There is near universal agreement that the ETT are generated by the partial melting of metabasic source rocks (Sen and Dunn 1994, Wolf and Wyllie 1994, Rapp and Watson 1995, Drummond et al. 1996, Nutman et al. 1999, Hoffmann et al., 2011, Hastie et al. 2016a), but the tectonic environment where this occurred is the subject of intense debate between primitive subduction zones (plate tectonics?) (Ernst et al. 2016; Nutman et al. 2009, 2015, Nutman and Friend 2009, Foley et al., 2014, Hastie et al. 2015, Polat et al. 2015, Kaczmarek et al. 2016, Ge et al. 2018) and a non-subduction (non-plate tectonic?) process (e.g., Robin and Bailey,

2009, Smithies et al. 2009, Thébaud and Ray, 2013, Zhang et al. 2013; Hawkesworth et al. 2016, Rozel et al., 2017; Wiemer et al., 2018). To complicate matters further, it is also argued that Archaean terranes show evidence of both horizontal tectonics (subduction or subcretion?) and vertical tectonics (Sizova et al. 2015; Bedard 2017) so that both tectonic regimes could have been operating at the same time. Furthermore, it has been suggested that subducting Archaean plates may have been weaker and may have broken up into drips as they descend (e.g., Moyen and van Hunen 2012). This process of weak plate subduction is termed dripduction (Moyen and Laurent 2018). Additionally, recent laboratory analogue experiments, numerical modelling and geological investigations of Earth and Venus, show that limited plume-induced subduction can initiate through slab roll back without active sea-floor spreading (Gerya et al. 2015, Davaille et al. 2017). This suggests that evidence of subduction on the early Earth may not indicate plate tectonics sensu stricto as subduction may occur in the absence of mid-ocean ridge volcanism.

Here, mass balance models are constructed using published data from high pressure-temperature (P-T) experiments to re-investigate ETT petrogenesis and examine if subduction processes or intracrustal melting of thick basaltic crust are responsible for forming the first continental landmasses ~4.0 Ga. Relatively recent studies have interpreted Eoarchaean terranes from a geologically holistic stance (e.g., Nutman and Friend 2009; Polat et al., 2015), but here we contribute to the debate by focussing on the petrogenesis of the ETT. It is important that the precise mechanisms responsible for early continental growth are known so that we can understand what elemental outputs and sinks they might have imparted onto primitive ecosystems and environments. This is fundamental because we cannot fully understand why all of the Earth's modern-day geochemical reservoirs have their present compositions and why life was able to evolve until we understand how the continents began to form.

2. Formation of ETT

It is generally accepted, based on high pressure-temperature (P-T) experiments and geochemical modelling, that the first continental materials (the ETT) were derived through partial melting of metamorphosed basic igneous protoliths (Sen and Dunn 1994, Wolf and Wyllie 1994, Rapp and Watson 1995, Winther 1996, López and Castro 2000, Foley et al. 2002, Rapp et al. 2003, Martin et al. 2005, Moyen and Stevens 2006, Adam et al. 2012, Laurie and Stevens 2012, Moyen and Martin 2012, Nagel et al. 2012, Zhang et al. 2013, Ziaja et al. 2014, Hastie et al. 2015, 2016a, Palin et al. 2016a). In contrast, proposed Eoarchaean tectonic environments in which the ETT were generated are extremely varied in detail, but broadly fall into two contrasting models.

Model 1 suggests that plate tectonic-like processes were absent in the Eoarchaean (Hamilton 1998, Van Thienen et al. 2004, Dhuime et al. 2012, Zhang et al. 2013, Kamber 2015, Hawkesworth et al. 2016, Rozel et al., 2017; Wiemer et al., 2018) and that the formation of the early continental crust occurred through intraplate partial melt processes after the Earth's magma ocean(s) had solidified, differentiated and formed a ~25-45 km thick stagnant basaltic lid. Published causal mechanisms for intraplate partial melting are diverse and can be interlinked (e.g., Sizova et al., 2015; Rozel et al., 2017), but are commonly attributed to: fusion of the base of the intraplate mafic crust due to upwelling of hot mantle (Zhang et al., 2013; Wiemer et al., 2018), heat pipes (Moore and Webb, 2013) or plutonic squishy lid tectonics (Rozel et al. 2017), crustal resurfacing (e.g., van Thienen et al., 2004), crustal overturn and sagduction (Robin and Bailey, 2009; Thébaud and Ray, 2013; Francois

et al., 2014; Sizova et al., 2015; Wiemer et al., 2018) or a crustal drip (with or without delamination, e.g., van Thienen et al., 2004; Sizova et al., 2015) (**Model 1, Fig.1**).

Model 2 requires that some sort of subduction was already underway in the Eoarchaean (and possibly >4.0 Ga) causing water from liquid oceans to be transported to depth in primitive flat/shallow subduction zones. In a process slightly different to present-day subduction the subsequent hydrous melting of thick basaltic subducting plates generated magmas with ETT compositions that solidified into the first continental crust (**Fig. 2b)** (Ernst et al. 2016; Harrison et al., 2005; Steenfelt et al., 2005; Hopkins et al. 2008; Chen et al., 2009; Nutman and Friend 2009; Jenner et al., 2009; Nutman et al., 2009, Foley et al., 2014, Polat et al., 2015; Hastie et al. 2016a, Kaczmarek et al., 2016) (**Fig. 1: Model 2**). Model 2 lacks a mantle wedge and would not generate the typical andesitic volcanism found in modern arc systems. However, small slivers of mantle material may have existed on the slab shear zone to give rise to small volumes of quartz diorite and andesite in the Eoarchaean rock record (Liu et al. 2007, Nutman et al. 2015). A variant of Model 2 involves Archaean subcretion tectonics whereby Eoarchaean continental drift would enable continents to push against thick Eoarchaean oceanic crust causing imbricated basaltic slabs that could melt to form silicic magmas (Bédard 2013, 2017).

Models 1 and 2 have both been, and continue to be, supported by a wide variety of field observations, geochemical data and numerical modelling so the debate on generating the first continents is ongoing. Here, we suggest that determining the most likely geodynamic make-up of the Eoarchaean Earth is best explored by undertaking a detailed petrological examination of the possible petrogenesis of ETT. A common approach for investigating the potential composition of the protoliths from which ETT are derived and their likely tectonic environment is to carry out high P-T partial melting experiments on materials with the composition of basic igneous rocks and determine if melts generated have similar compositions to the first silicic crust (Beard and Lofgren 1991, Rushmer 1991, Sen and Dunn 1994, Wolf and Wyllie 1994, Patiño Douce and Beard 1995, Rapp and Watson 1995, Skjerlie and Patiño Douce 1995, Winther 1996, Springer and Seck 1997, López and Castro 2000, Skjerlie and Patiño Douce 2002, Rapp et al. 2003, Adam et al. 2012, Laurie and Stevens 2012, Zhang et al. 2013, Ziaja et al. 2014, Hastie et al. 2016a). Unfortunately, individual experimental studies on a range of metabasic compositions [e.g., mid-ocean ridge basalt (MORB) and island arc] and lithologies (amphibolites and eclogites) have not yet fully replicated the major- and trace-element characteristics of ETT (Beard and lofgren 1991, Rushmer 1991, Sen and Dunn 1994, Wolf and Wyllie 1994, Patiño Douce and Beard 1995, Rapp and Watson 1995, Skjerlie and Patiño Douce 1995, Winther 1996, Springer and Seck 1997, López and Castro 2000, Skjerlie and Patiño Douce 2002, Rapp et al. 2003, Adam et al. 2012, Laurie and Stevens 2012, Zhang et al. 2013, Ziaja et al. 2014, Hastie et al. 2016a). Nevertheless, all of the high P-T experiments have produced major element data for the resulting partial melts and, if all of these previous experiments are taken together as a single group, they generate magma compositions with such a wide major-element variability that they encompass all of the ETT compositions. In contrast, assessing the trace element variability of previous high P-T experiments is difficult because very few studies present trace element analyses of experimentally derived melt (Rapp et al. 1999, Adam et al. 2012, Laurie and Stevens 2012, Hastie et al. 2016a). Of those that do, the partial melting of metabasic MORB (Laurie and Stevens 2012), back-arc basalt (Rapp et al. 1999), Hadean greenstone (Adam et al. 2012) and oceanic plateau basalt (Hastie et al. 2016a) all generate magmas that approach ETT compositions – especially the oceanic plateau-derived melts.

Major element analyses of experimentally derived melts are useful for determining if a partial melt from a particular protolith matches the earliest continental material because ETT have distinctive major element contents relative to other granitoids (Drummond et al. 1996,

Martin et al. 2005, Kamber et al. 2002, Nutman et al. 2009, Hoffmann et al. 2011, 2014, Ge et al. 2018). For example, compared to modern granites, Archean TT(G) have low K_2O- and very high Na_2O contents leading to low K_2O/ Na_2O ratios of ~0.4 (granites are typically >0.8) (Martin et al. 2005, Nutman et al. 2009, Hoffmann et al. 2011, Moyen and Martin 2012) (**Fig. 2a**). Importantly, ETT also have a very distinctive trace element composition compared to other granitoids and younger TTG (Condie 2005, Martin et al. 2005). Most TT(G) have strongly fractionated rare earth elements (REE) (expressed as high La/Yb), characteristically high Sr/Y ratios and low heavy (H)REE concentrations (Drummond et al. 1996, Kamber et al. 2002, Martin et al. 2005, Nutman et al. 2009, Hoffmann et al. 2011, 2014, Ge et al. 2018) (**Fig. 2b)**. However, ETT typically have higher Ba contents and lower Sr and transition element abundances than do younger TT(G) (Martin and Moyen 2002, Martin et al. 2005) (**Fig. 2c**). Trace element concentrations and patterns are arguably more sensitive to different geological processes and more useful for determining the petrogenesis of an igneous rock than are major elements. Unfortunately, analysing the trace element abundances of experimentally derived phases is technically difficult and these are rarely reported. Nonetheless, it is known that the distinct trace element abundances and patterns seen in Archaean TTG (**Figs. 2b and 2c)**, are generated in metabasic-derived partial melts by (1) the compositional diversity of the protolith (e.g., Adam et al. 2012, Laurie and Stevens 2012) and (2) modally variable residual mineral phases buffering and/or fractionating trace elements [e.g., Sr is compatible in plagioclase (Martin et al. 2005), the HREE are compatible in garnet (Sen and Dunn 1994) and Nb is compatible in rutile (Klemme et al. 2002)]. However, there are far too few actual trace element analyses from high P-T experiments to explore all of the complex trace element concentrations and patterns from ETT. Hence, in order to better understand how the compositionally unique ETT formed we have to undertake trace element modelling to identify the most likely starting protolith and residual mineralogy. If the modelling is successful, it may be possible to determine what tectonic environment(s) gave rise to the first continents and establish the geodynamic make-up of the early Earth.

3. Modelling Methodology

3.1 Current approach

A number of recent studies (e.g., Nagel et al. 2012, Palin et al. 2016a, Johnson et al. 2017) have used computer programs based on phase equilibria (e.g., THERMOCALC) to model the derivation of TT(G) and have presented evidence in favour of intracrustal and/or subduction models. Our methodology is different in that we collate the mineral and melt modes of previous high P-T experiments and use mass balance to calculate the composition of the liquids generated. Previous experiments have used a variety of starting compositions [MORB (Winther 1996, López and Castro 2000, Laurie and Stevens 2012), arc (Beard and lofgren 1991, Rushmer 1991, Adam et al. 2012), oceanic plateau (Hastie et al. 2016a), greenstone (Adam et al. 2012), alkali basalt (Rushmer 1991) and a range of synthetic (Archaean) material (Patiño Douce and Beard 1995, Zhang et al. 2013, Ziaja et al. 2014)]. A range of initial and/or residual mineral assemblages [amphibolites (Rushmer 1991, Sen and Dunn 1994, Wolf and Wyllie 1994, Patiño Douce and Beard 1995, López and Castro 2000, Zhang et al. 2013) and eclogites (Sen and Dunn 1994, Laurie and Stevens 2012)] at a range of temperatures and pressures (790-1225°C and 0.1-3.2 GPa) at anhydrous to hydrous conditions (up to 32 wt.% water, Laurie and Stevens 2012) have also been used to generate silicic liquids. The many experimental results give us the actual modal residua-mineral and melt proportions over a P-T-X range that most likely encompasses the conditions required to derive ETT from an intracrustal and/or subduction environment.

The experimental data are invaluable because, if we know the melt fraction *(F)*, the modal proportion of residual equilibrium phases, and the distribution coefficient (*D*) between the

residual solid and the melt, it is straightforward to calculate the liquid composition by mass balance

$$C_0 = FC_L + (1-F)C_R \qquad [1]$$

where C_0 is the initial concentration of some element in the experimental starting material, C_L its concentration in the melt and C_R its concentration in the residual phases. By definition

$$C_R = DC_L \qquad [2]$$

and substituting [2] in [1] and rearranging gives

$$C_L = \frac{C_0}{D + F(1-D)} \qquad [3]$$

which is Shaw's (1970) modal melting equation. Thus, we only need to know the initial bulk composition, the residual mineral assemblage, their respective solid/melt distribution coefficients, and the melt fraction in order to estimate the melt composition. The starting (un-melted) metabasic protolith composition (C_0) will be varied to see which protolith can best explain the ETT data. Here we use modern MORB, oceanic plateau basalt, theoretical Eoarchaean oceanic crust and Eoarchaean arc-like protoliths. The bulk distribution coefficient (D) appropriate to each residual assemblage is calculated from the modal mineral proportions reported in high P-T experimental studies and partition coefficients for the individual mineral phases. We use the partition coefficients given by Bédard (2006) because these are very widely used in the recent literature (e.g., Hastie et al. 2015, Johnson et al. 2017). F (melt fraction) is the modal melt proportion reported in individual experiments. It is important to note that the modal proportions used in these mass balance calculations have to be in weight percent and not volume or mole percent. The only assumption we make is that the experiments have all reached equilibrium.

In carrying out our calculations we assume that melts are produced by batch (equilibrium) melting in which melt remains in contact with residual solid until the final melt fraction F is reached. This approach is required because we base our calculations on the results of melting experiments in which melt and solid phases remain in equilibrium. However, partial melting in the Earth is better described by a fractional melting process in which melt is drained continuously as it forms and therefore does not remain in equilibrium with residual solid phases throughout the melting process. To model fractional melting requires knowledge of the initial proportions of each mineral phase (the phase mode) and the proportion that each phase contributes to the melt (the melt mode). We could then use Shaw's (1970) equation for perfect fractional melting to calculate the composition of the accumulated melt. Fractional melting produces concentrations of incompatible elements that are up to 30% higher than those from batch melting because fractional melting is more efficient at stripping the more incompatible elements from the source. The maximum difference between the two models is found when F≈D and so ratios between highly incompatible and moderately compatible elements are likely to be the most affected by choice of model. We have calculated the magnitude of the difference between batch and fractional melting by estimating the phase and melt modes from some of the experiments (not all studies give enough information for us to work out the phase and melt modes) and then using Shaw's (1970) equation for accumulated fractional melt to calculate the concentrations of a wide range of elements in melts formed from a normal (N)-MORB source. As we will show later, the calculated differences are too small to affect our conclusions and so we will use the more robust batch-melting approach here.

3.2 Oceanic plateau starting composition

It can be argued that the first stable and survivable continents, regardless if they were generated from primitive subduction zones, subcretion or intracrustal environments, are most likely derived from a protolith with basaltic oceanic plateau-like compositions. Mesozoic oceanic plateaus (e.g., Ontong Java Plateau and the Caribbean Oceanic Plateau) were generated by the partial melting of hot mantle in plume heads, and are composed of basaltic crust up to 20-35 km thick that is less incompatible element depleted than N-MORB (Herzberg and O'Hara 2002, Fitton and Godard 2004, Herzberg et al. 2007, Kerr et al. 2014, Herzberg and Asimow 2015, Hastie et al. 2016b).

In the Hadean the Earth initially had a magma ocean(s) that solidified and differentiated into basaltic crust (Elkins-Tanton 2008). This first crust may have been mostly destroyed during the Late Heavy Bombardment (LHB) ~3.8-4.1 Ga (Gomes et al. 2005, Kamber 2015), but the basaltic crust that survived, and formed afterwards, was probably 25-45 km thick and would have had a composition similar to Mesozoic oceanic plateaus (e.g., the non-arc basalts of Herzberg et al. 2010). Archaean mantle plume-derived komatiites do exist alongside non-arc basalts, but they are volumetrically minor (<5%) and are not representative of Eoarchaean crust (Herzberg et al. 2010; Johnson et al., 2014). Therefore, if ETT was derived by intracrustal melting, it was likely Mesozoic oceanic plateau-like material that melted. Conversely, if plate tectonic-like processes existed on the Eoarchaean Earth (Model 2), then crust formed at Eoarchaean spreading centres might have been a plausible protolith from which to generate the first continents through metamorphism and melting in an Eoarchaean subduction setting. Eoarchaean upper mantle was hotter and less depleted in incompatible elements than the present-day asthenosphere (Shirey et al. 2008, Herzberg et al. 2010). Thus, Eoarchaean spreading centres should have been characterised by larger degrees of partial melting, producing less depleted and thicker oceanic crust (~30-45 km) than today (~7 km) (Abbott et al. 1994, Smithies et al. 2003, Herzberg et al. 2010, Moyen and Martin 2012, Bedard 2017). The lack of continental crust before ~4 Ga, would have meant that this thick oceanic crust would have been the dominant surface rock type (Kamber 2010, Dhuime et al. 2015, Tang et al. 2016), making it a likely protolith from which to derive Eoarchaean continents. As no definitive Eoarchaean oceanic crust has survived to be examined (e.g., Nutman et al., 2009) the closest analogue in terms of thickness and geochemistry, if not mode of formation, are the Mesozoic oceanic plateaus. This is supported by a geochemical study by Reimink et al. (2014) on a ~4.0 Ga mafic tonalite in Canada that has been interpreted as forming in an oceanic plateau (Iceland-like) environment.

Hastie at al. (2016a), set out to replicate the composition of Eoarchaean silicic crust by carrying out high P-T experiments using a single sample of Mesozoic Ontong Java Oceanic Plateau (OJP) Kroenke-type basalt, which is anhydrous, primitive and relatively depleted [e.g., high MgO and low TiO_2, light (L)REE, Th and U (Fitton and Godard 2004)]. This study also simulated a primitive subduction environment, and since a shallow subducting slab is converted to an amphibolite with ~1-3 wt. % water (Peacock et al. 1994, Kogiso et al. 1997, Tatsumi and Kogiso 1997), a similar amount of water was added to the anhydrous OJP experimental starting material. Hastie et al's (2016a) experiments were run from 1.6-2.2 GPa and 825-1000°C and generated tonalite-composition liquids in equilibrium with plagioclase- and garnet-bearing amphibolites that lacked residual rutile (low TiO_2 content prevents rutile stabilising). Almost all elements from the OJP-derived tonalites match ETT compositions; however, the OJP experimental liquids have low K_2O and Ba contents relative to the ETT data compiled by Nutman et al. (2009), Hoffmann et al. (2011, 2014), Kamber et al. (2002) and Ge et al. (2018) (**Fig. 3a**). Furthermore, ETT commonly have pronounced negative Nb-Ta anomalies on N-MORB normalised multielement diagrams whereby ETT have (La/Nb)nmn (N-MORB normalised) ratios of 0.6-49.8. The OJP-derived melts overlap the

ETT with (La/Nb)nmn of 0.7-2.3, but require either enrichment of the LREE and/or residual rutile (partition coefficients for Nb and Ta >>1) in order to increase the (La/Nb)nmn ratio (Hastie et al. 2016a) (**Fig. 3a**). As no rutile was stabilised in the OJP experiments, Hastie et al. (2016a) increased the incompatible element contents and the (La/Nb)nmn ratio of the OJP-derived melts by assuming that the melts mix with dehydration fluids released from deep within a subducting slab (**Fig. 1: Model 2**). The modelled OJP-derived partial melt + slab fluid mixtures have compositions that match a larger portion of, **but not all**, the ETT because the slab fluid increases the contents of the incompatible elements (K_2O, Ba and LREE) in the mix (**Fig. 3b**). Nevertheless, although an OJP-derived melt and slab fluid mixture can explain some of the ETT compositions, a few questions remain:

1. Can oceanic plateau material that has higher incompatible element contents and high enough TiO_2 to stabilise residual rutile undergo partial melting to generate liquids (with or without a slab fluid) with compositions that can explain all ETT-like compositions?
2. Can intracrustal melting of oceanic plateau material with high incompatible element and TiO_2 contents at low pressures (≤1.4 GPa: maximum base of thick mafic crust) generate ETT like compositions without the need for a slab-fluid?

3.3 Possible slab flux components

The OJP-derived tonalite melts reported by Hastie et al. (2016a) have compositions that match a proportion of ETT only by mixing them with a hypothetical slab-derived fluid component. As such, it may be possible that melts derived from the fusion of different metabasic protoliths could be mixed with similar slab fluids to generate all ETT-like compositions. Therefore, a slab component can be used in our models to explore all options for forming the ETT. The composition of a slab-derived fluid is calculated by using the methodology of Kogiso et al. (1997) who studied dehydration processes experimentally on a natural amphibolite under open system conditions. Kogiso et al. (1997) define the mobility of an element as

$$E_m = \frac{C_0 - C_{fl}}{C_0} \qquad [4]$$

where E_m is element mobility, C_0 is the element concentration in a starting amphibolite and C_{fl} is the concentration of an element in the amphibolite after fluid loss. The concentration of an element in a slab-derived fluid is then calculated based on the extracted water content in the altered slab by

$$C_{sf} = \frac{C_0 P E_m}{X_{H2O}} \qquad [5]$$

Where C_{sf} is the element concentration in the slab-derived fluid, C_0 is the concentration of the element in the starting rock unit(s), P is the proportion that the rock unit(s) contribute to the slab fluid concentration, and X_{H2O} is the mass fraction of water. The final composition of a combined ETT melt and slab-fluid mixture can be determined using mass balance

$$C_m = C_{ETT}(1 - X) + C_{sf}X \qquad [6]$$

where C_m is the concentration of an element in a mixture of ETT (C_{ETT}) with an added fraction (X) of the slab-derived component (C_{sf}).

3.4 Eoarchaean metabasaltic rocks with island-arc affinities

Field observations in Archaean terranes (Polat et al., 2015), previous geochemical studies (Nutman et al. 1999, Hoffmann et al. 2011, Adam et al. 2012, Hastie et al. 2015, O'Neill et al. 2016, O'Neill and Carlson 2017, Cox et al. 2018) and phase equilibria modelling (Nagel et al. 2012, Hoffmann et al. 2014, Johnson et al. 2017, Ge et al. 2018) suggest that ETT could also be derived from the partial melting of Eoarchaean metamorphosed mafic crust with a chemical composition similar to that of present-day island arcs (e.g., negative Nb anomalies on multielement diagrams) (e.g., Jenner et al. 2009, Hoffmann et al. 2011). Some studies also suggest that these arc-like mafic protoliths are, themselves, possibly derived from the partial melting a mafic crustal precursor so that ETTs are derived through a multi-stage petrogenetic process (Johnson et al. 2017). Fusing of Eoarchaean arc-like metabasic rocks has been suggested to occur in both an intraplate (Hoffmann et al., 2011, Cox et al. 2018) and subduction environment (Ge et al., 2018). However, if this were the case then subduction similar to that on the modern Earth may have been operating before the formation of the earliest ETT crust. Therefore, Eoarchaean rocks with island arc-like compositions remain a plausible protolith from which to derive the earliest TTG and this leads us to a follow up question from those in section 3.2:

3. Can partial melting of Eoarchaean island arc-like crust generate ETT like compositions?

3.5 Which trace elements should we model?

3.5.1 Investigating a slab fluid

One of the key geochemical characteristics of ETT is a negative Nb-Ta anomaly on N-MORB normalised multielement diagrams (**Fig. 3a,b)** (Nutman et al. 1999, 2009, Kamber et al. 2002, Hoffmann et al. 2011, 2014, Ge et al. 2018). This anomaly can either be explained by residual rutile in a metabasic source region (partition coefficients for Nb and Ta in rutile are ~40-70: Bédard 2006) and/or mixing a metabasic-derived partial melt with a slab fluid that is enriched in large ion lithophile elements (LILEs), LREEs, Th and U relative to Nb and Ta. Resolving whether residual rutile and/or a slab fluid are responsible for the negative anomalies in ETT is key to determining whether a subduction or an intraplate environment is dominantly responsible for ETT generation. An intraplate environment on an early Earth, that lacked a plate tectonic regime would have to be able to stabilise rutile at relatively low pressures (<0.8-1.4 GPa; <25-45 km) if the mafic crust undergoes *in situ* partial fusion to form ETT magmas (Kamber 2015, Hawkesworth et al. 2016, Palin et al. 2016). However, higher pressures can be invoked if ETT magmas are derived from lithospheric drips/delamination in an intracrustal regime. In order to determine if both residual rutile and a slab fluid are required to generate the full range of negative Nb-Ta anomalies seen in the ETT, trace element ratios in which the numerator element is transported in a slab fluid (e.g., K/Y and La/Y) or retained in residual rutile (Nb/Y) will be used in our models.

3.5.2 A depth investigation using plagioclase (Sr), Garnet (HREE) and Rutile

It is well documented in the literature that the stability of plagioclase and garnet in a metabasic igneous rock is highly pressure dependent, with plagioclase stable at low pressures and garnet at high pressures (Martin et al. 2005, Xiong et al., 2005; Moyen and Stevens 2006). The exact pressure at which plagioclase is replaced by garnet is dependent on the temperature and composition of the system, but commonly, garnet is considered to be stable deeper than ~30 km (~1 GPa) (Beard and Lofgren 1991, Wolf and Wyllie 1994, Springer and Seck 1997, Zhang et al. 2013) and plagioclase can exist up to ~55 km (~1.6-1.8 GPa) (Sen and Dunn 1994, Wolf and Wyllie 1994, Patiño Douce and Beard 1995, Winther 1996, Springer and Seck 1997, Martin et al. 2005, Moyen and Stevens 2006, Zhang et al. 2013,

Hastie et al. 2016a). Strontium is compatible in plagioclase and the HREEs are compatible in garnet (Bédard 2006). Thus, Sr and the HREE can be used, as in other studies (Van Hunen and Moyen 2012), to investigate the depth from which ETT are derived. Rutile stability is also pressure dependent and experimental studies show that it is stable above ~40-50 km depth (1.25-1.50 GPa) in a basaltic protolith (Patiño Douce and Beard 1995, Xiong et al. 2005). In order to explore the changing mineralogy with depth, trace elements that would only be affected by residual plagioclase (e.g., Sr) and garnet (e.g., Y and the HREE) will be used in our models.

4. Results and Discussion

Tables 1-4 show a worked numerical example where the trace element concentration of partial melts from experimental runs reported by Hastie et al. (2016a) are calculated by mass balance calculations. The calculated melt compositions in Table 4 have similar trace element concentrations and patterns on N-MORB normalised multielement diagrams to actual partial melt analysed by Hastie et al. (2016a) (**Figs. 3a and c**). In particular, the positive Ba and negative Ti anomalies are replicated in the models. Also, as with the actual analyses, modelled partial melts calculated for experiments with residual plagioclase show low Sr concentrations relative to experiments with residual garnet, which show lower abundances of the HREE. As a consequence, because the compositions of the modelled melts match the analytical data so well, we think that the variables used in our calculations are appropriate. Unfortunately, a much wider comparison between actual analyses and modelled partial melt compositions cannot be undertaken because of the lack of published data.

4.1MORB as a starting composition: testing the model

Figures 4a and **4b** show plots of K/Y-Nb/Y in which fields for MORB, OIB and oceanic plateau basalt data define a 'mantle array' beneath island arc and ETT data fields. In calculating our theoretical MORB-derived partial melts we use the N-MORB starting composition of Hofmann (1988). The melt compositions shown in **Figure 4a** (yellow and green circles) were calculated by assuming batch melting *only* (equation [3]) whereas those in **Figure 4b** (yellow and cyan triangles) were calculated with Shaw's (1970) batch and accumulated fractional melting equations respectively, as outlined in section 3.1. The batch melt compositions in **Figure 4b** are yellow triangles (as opposed to yellow circles as in **4a**) because the batch melt trend in **4b** is constructed with less samples than in **4a** due to some experimental studies not publishing enough data to be able to calculate accumulated fractional melts for direct comparison to their batch melt counterparts. The differences in the two sets of calculated melt compositions (batch vs. accumulated fractional) is small and so the melt compositions shown in all subsequent figures (apart from **4g**) are based on batch melting calculations. Batch melting is our preferred melting model because our melt compositions are based on batch melting experiments and we can construct the melt trends with more data points.

In Figure 4a our calculated partial melts from a metabasic source of N-MORB composition form a linear melt array (yellow circles) that extends from low K/Y and Nb/Y values in the MORB field and passes through the oceanic plateau and OIB fields. The only compositions that deviate from the main trend are from the experimental runs that have residual rutile (highlighted as green circles). The presence of residual rutile with our N-MORB source composition is justified as the TiO_2 content of the protolith is ~2.0 wt. %. (e.g., Klemme et al. 2002). We increased the original TiO_2 concentration of 1.615 wt.% to 2.0 wt.% because the experimental residual mineral modes can have up to 2.0 wt.% rutile (although in natural systems amphibole would take a considerable amount of TiO_2: Xiong et al., 2005). The calculated partial melt compositions derived from source regions with residual rutile are

displaced to lower Nb/Y contents at a given K/Y value. In addition to the calculated melt compositions, actual analyses of partial melts derived from hydrous MORB-like eclogite starting compositions reported by Laurie and Stevens (2012) are also plotted (black circles).

In **Figure 4a**, our calculations show that partial melts derived from metabasic sources with an N-MORB composition do not plot in the ETT field. Niobium has a high partition coefficient between rutile and silicic liquid, which explains why partial melts derived from rutile-bearing residues are displaced to lower Nb/Y. Conversely, calculated partial melt compositions on Th/Y-Nb/Y, La/Y-Nb/Y and Sr/Y-Nb/Y diagrams do plot in the ETT field, but only do so in the La/Y-Nb/Y diagram if residual rutile is present at pressures >1.25 GPa (**Figs. 4c-e**).

Calculated metabasic-derived partial melt trends in the K/Y-Nb/Y diagram suggests that the presence of rutile by itself cannot generate ETT-like compositions by fusing an N-MORB protolith. This is confirmed in a K/Y-Zr/Y diagram (also a Ba/Y-Zr/Y diagram; not shown) which shows that calculated partial melt compositions also do not plot in the ETT field (**Fig. 4f**). We again show a comparison of batch vs. accumulated fractional melts in **Figure 4g** to demonstrate the similarity of the results using the two partial melt equations. The K/Y-Zr/Y diagram is important because the presence of residual rutile has little effect on the melt trend due to the relatively low D values of K, Y and Zr between rutile and silicic melt (Bédard 2006). Therefore, even N-MORB sources with higher modal proportions of rutile cannot be melted to reproduce the ETT K/Y-Zr/Y ratios (we shall discuss alteration processes in a later section). In contrast, La/Y and Th/Y-Zr/Y diagrams have partial melt trends that do intersect the ETT field (**Figs. 4h and i**).

4.2 Oceanic plateau basalt as a starting composition

Calculated batch partial melt compositions are shown in **Figures 5a-g** using a primitive high MgO oceanic plateau basalt from the Ontong Java Plateau (OJP) as a starting composition (KR1187-8: Fitton and Godard 2004). This sample was used by Hastie et al. (2016a) as the starting material in high-P-T laboratory experiments to replicate ETT magmas. Like the N-MORB results, modelled oceanic plateau-derived metabasic silicic melts form melt trends from rutile-free residues that do not intersect the ETT field in K and La/Y-Nb/Y diagrams (**Figs. 5a and c**). However, modelled melts from source regions with residual rutile plot in the ETT field in the La/Y-Nb/Y diagram and in the extreme lower parts of the ETT field in the K/Y-Nb/Y diagram (**Figs 5a and c**). Modelled melts, with or without residual rutile, also plot in the ETT fields on Th/Y-Nb/Y and LILE and LREE/Y-Zr/Y diagrams (although only a few samples do so in the K/Y-Zr/Y plot) (**Figs 5a-g**).

Overall, **Figure 5** suggests that melting a metamorphosed igneous protolith with an oceanic plateau composition can generate some ETT-like melts if residual rutile is present. Nevertheless, the experimental work in Hastie et al. (2016a) demonstrate that rutile is not a residual phase in primitive oceanic plateau starting compositions, even at 2.2 GPa. The KR1187-8 starting composition has a TiO_2 content of ~0.75 wt.% and previous experimental work on eclogites suggests that rutile may not saturate unless the TiO_2 composition of the starting protolith is >1.0 wt.% (Klemme et al. 2002). Additionally, 0.75 wt.% TiO_2 is not enough TiO_2 to form the high modal rutile abundances in some of the experimental studies (e.g., Patino Douce and Beard, 1995). This led Hastie et al. (2016a) to invoke a mixture of oceanic plateau-derived slab melt and slab-fluid to explain the composition and petrogenesis of ETT. **Figures 5a-g** show trace element data from analysed melt pools in the oceanic plateau fusion experiments of Hastie et al. (2016a) (orange circles). The analysed melt pools plot along the main modelled melt trends in all trace element ratio diagrams. Tables 1-4 show the procedure by which we calculated the composition of a slab-derived fluid from a hypothetical subducting section of OJP-like crust. Hastie et al. (2016a) originally used simple

mass balance to suggest that a mixture of 4% slab fluid and 96% slab melt can generate ETT-like magmas. Tables 1-4 show a slight modification of this mass balance analysis whereby the calculations are applied to more elements (e.g., Na). To be consistent with Hastie et al. (2016a) a mixture of 4% slab fluid and 96% slab melt is once again assumed for each of the experimental OJP-derived slab melt analyses (blue circles). **Figure 6** shows that the major and trace element compositions of these mixtures (calculated as shown in Tables 1-4) have compositions almost identical to ETT. On **Figures 5a-g** the oceanic plateau-derived slab melts and slab fluid mixtures plot in the ETT fields, although the mixtures only plot in small parts of the ETT field in the K/Y-Nb/Y diagram. Thus, the addition of a slab fluid to an oceanic plateau-derived slab melt can explain some, but not all, of the ETT data.

4.3 Are both rutile and a slab fluid needed to generate most of the ETT?

Rutile or a slab fluid individually cannot account for high ETT-like K/Y, Th/Y and La/Y ratios at a given Nb/Y value in our initial models (**Fig. 5**). However, it is likely that melting a metamorphosed oceanic plateau-like protolith could generate the whole range of ETT compositions if both rutile and a slab fluid are involved in the petrogenesis. As such, it is possible that a more differentiated and/or enriched oceanic plateau-like protolith with higher TiO_2 contents could stabilise rutile as a residual phase. If a partial melt derived from this more differentiated and/or enriched protolith also mixed with a slab fluid during ascent the resultant mixtures may explain the whole ETT compositional field. However, even though Mesozoic oceanic plateaus are the best modern-day analogues for possible Eoarchaean oceanic crust, the Mesozoic mantle plumes that they were derived from are generated from partial melting mantle material that is relatively depleted in incompatible elements compared to the more primitive mantle of the Eoarchaean Earth because of the extraction of continental crust over geological time (Fitton and Godard 2004, Dhuime et al. 2015, Moyen and Laurent 2018). As a result, Eoarchaean upper mantle was probably more similar in composition to primitive mantle and would have undergone large degrees of partial melting to form thick oceanic crust that was relatively enriched in the more incompatible elements compared to Mesozoic oceanic plateau crust.

Undepleted mantle source regions, similar in composition to pyrolite estimates, can generate 30% partial melts with major element contents identical to oceanic plateau primary melts (McDonough and Sun 1995, Walter 1998, Herzberg et al., 2007, Herzberg and Asimow 2015). Oceanic plateau primary melts differentiate to primitive magmas through approximately 30% olivine fractional crystallisation (Korenaga and Kelemen 2000, Fitton and Godard 2004, Herzberg et al., 2007, Herzberg and Asimow 2015, Hastie et al. 2016b). More evolved oceanic plateau basaltic lavas are produced by subsequent crystallisation of plagioclase and clinopyroxene (Korenaga and Kelemen 2000, Fitton and Godard 2004). Fitton and Godard (2004) estimate that differentiated OJP lavas are derived by up to 50% fractional crystallisation of a cotectic assemblage of 0.15 olivine, 0.25 clinopyroxene and 0.6 plagioclase after initial olivine crystallisation. Consequently, we have calculated the composition of two theoretical differentiated Eoarchaean basaltic crustal source regions by assuming (1) 30% partial melting of a primitive mantle source region to form a primary magma, (2) 30% fractional crystallisation of olivine from the primary magma to form a primitive basaltic liquid and (3) either 20 or 50% fractional crystallisation of the primitive magma to form a differentiated basalt using the crystallising mineral modes of Fitton and Godard (2004).

We calculated the composition of silicic melts derived from the two Eoarchaean oceanic crust protoliths by using (1) the two theoretical Eoarchaean differentiated basalts as the starting compositions and (2) the modal mineral and melt proportions from the oceanic plateau-derived experiments in Hastie et al. (2016a). However, because the theoretical

differentiated basaltic source regions have ~1.0 and 1.6 wt.% TiO_2 with 20% and 50% fractionation of the cotectic assemblage respectively, we modified the oceanic plateau mineral modes to include 0.75 wt.% rutile. The amount of rutile would probably increase as pressure increases (e.g., Xiong et al., 2005), but to keep the models simple we kept the modal proportion constant. The use of a theoretical differentiated basalt, as opposed to the primitive Kroenke-type basalt in Hastie et al. (2016a), would result in slightly different residual mineral modes. However, we assume that the bulk residual mineral assemblies do not substantially change and would not bring about large compositional shifts on the bivariate plots that we have previously used. For example, our plots use Y as a denominator so slight differences in garnet abundance should just more the partial melt trends long a trend parallel to our 'mantle' or 'arc-ETT' arrays. Additionally, there are several igneous processes that may modify the composition of our modelled Eoarchaean silicic melts that we also need to address. These processes include: (1) for a potential subduction environment, possible partial melting of sedimentary rocks on an Eoarchaean slab shear surface, (2) near-surface alteration of the metabasic protolith affecting highly mobile elements, (3) extensive fractional crystallisation of the silicic melts on ascent and (4) assimilation of pre-existing shallow continental crust into the evolving silicic magma.

Previous studies on ETT use major and trace element geochemistry to suggest that the ETT are near primary silicic liquids and have not undergone extensive fractional crystallisation (Nutman et al. 1999, 2009). Trace element and Sr-Nd-Pb radiogenic isotope geochemistry also show that ETT magmas are near-primary melts and have not been modified by pre-existing crustal material (Nutman et al. 1993, Kamber et al. 2002, O'Neill et al. 2007, Nutman and Friend 2009, Hiess et al. 2009). $\delta^{18}O$ data from zircons in ETT are lower than 6.5‰, which indicates that primary ETT magmas are not derived from, or have not been significantly contaminated by, source regions represented by low-moderate temperature (0-100°C) altered continental crust, oceanic sediments or altered shallow oceanic crust (Hiess et al. 2009). This suggests that if ETT magmas are derived from a metabasic source in a primitive subduction zone any sedimentary veneer and the uppermost mafic section of the plate must have been scraped off during shallow subduction (Hiess et al. 2009). Conversely, the ETT have $\delta^{18}O_{Zr}$ on the low end of zircon mantle values which suggests that ETT could be generated with a mafic source component that has been hydrothermally altered at high temperatures (20% by mass balance) (Hiess et al. 2009). Therefore, in our mass balance calculations, we model the effects of limited hydrothermal alteration of the Eoarchaean basaltic source region and limited fractional crystallisation of the silicic melts at low and high pressures.

Figures 7a-g show the results of melting a theoretical Eoarchaean differentiated basalt generated with 20% fractionation of the cotectic assemblage, with rutile as a residual phase, and then mixing the resulting silicic melts with a calculated slab fluid (light blue circles). Again, the mixing ratio is 96:4 from Hastie et al. (2016a), but the results can be replicated with a wide variety of mixing percentages. **Figures 8a-g** replicate **Figures 7a-g**, but the theoretical Eoarchaean differentiated basalt is generated with 50% fractionation of the cotectic assemblage and has a higher TiO_2 content. In both **Figures 7 and 8**, the calculated melts plot in the ETT fields in all diagrams, although only in the extreme lower part of the ETT field in the K/Y-Nb/Y diagram. We then model several fractional crystallisation trends that involve a low pressure assemblage (Plagioclase: 0.743, Amphibole: 0.215, Magnetite: 0.042 (Macpherson et al. 2006), a high pressure assemblage (Amphibole: 0.1745, Clinopyroxene: 0.5296, Orthopyroxene: 0.1725, Garnet: 0.1234 (Macpherson et al. 2006) and amphibole only (Nutman and Bridgewater 1986, Hastie et al. 2015). We model 10% fractional crystallisation to generate the range of calculated melts in **Figures 7 and 8** (dark blue, dark red and light green circles). The fractional crystallisation trends are very similar to

the compositions of the primary silicic melt + slab fluid mixtures (light blue circles) and plot in the ETT fields also. The only remaining misfit is that all of the calculated melt compositions plot in the extreme lower part of the ETT field with regards to K/Y (**Figs. 7a, e and 8a, e**).

Potassium concentrations are commonly increased markedly in igneous rocks because of secondary alteration processes (Fitton and Godard 2004, Hastie et al. 2007). Altered OJP samples with high loss on ignition (LOI) values can have K_2O as high as 1.4 wt.% (sample 803-2, Fitton and Godard 2004). K/Y ratios of silicic melt + slab fluid mixtures in **Figures 7a, e and 8a, e** are presented that represent a mass balance mixture between 80% of our theoretical Eoarchaean oceanic crust protoliths (0.166 and 0.253 wt.% K_2O with 20 and 50% cotectic fractionation respectively) and 20% of altered oceanic crust with 1.4 wt.% K_2O (80:20 ratio was used as it is consistent with the oxygen isotope data: dark green circles). The new modelled melts plot much higher in the ETT field on the K/Y-Nb/Y and K/Y-Zr/Y diagrams. The case for high levels of K enrichment due to alteration, even higher than the value used in our modelling here, can be made because the early hydrosphere may have been significantly more saline than today (see Knauth 2005 for a review).

The modelled melts in **Figures 7 and 8** demonstrate that ETT can be generated by (1) the partial melting of slightly altered and differentiated metabasic Eoarchaean crust in the presence of residual rutile, (2) the mixing of these silicic slab-derived melts with a slab fluid component, and (3) limited fractional crystallisation of the ascending slab melt + slab fluid mixtures as they ascend through overlying mafic crust. It should, however, be noted that Jenner et al. (2009) suggest that >3.8 Ga 'enriched' mafic amphibolites with island arc-like compositions from the Isua Supracrustal Belt, Greenland are derived from a primitive Eoarchaean subduction zone and that their geochemistry can be partly explained with the addition of a sedimentary slab-derived component. Therefore, it may be possible to increase the K/Y ratios of some ETT if a sedimentary component is involved in their petrogenesis. Likewise, if the Eoarchaean oceans were more saline than today (Knauth 2005), slab-derived fluids may impart higher K contents to ETT source regions.

4.4 Eoarchaean arc-like starting composition

Major and trace element concentrations can be quite variable in Eoarchaean arc-like mafic rocks and it is difficult to decide on a single starting composition. However, the >3.8 Ga amphibolitised basalts with arc-like signatures from the Isua Supracrustal Belt analysed by Jenner et al. (2009) are categorised into a 'normal' group and an 'enriched' group. We use the averages from both the 'normal' and 'enriched' group as starting compositions in **Figures 9 and 10** respectively. However, the former and the latter have average TiO_2 contents of 0.82 and 0.94 wt.% respectively. Many of the high P-T experimental mineral residues have ≥1.0 wt.% rutile. Therefore, in order to use these experiments in our calculations we assume that the Eoarchaean arc like protoliths have ~1.0 wt.% TiO_2, and we have removed the experimental data that are generated with higher residual rutile. **Figures 9a-g** show that the modelled melts with no residual rutile easily intersect the ETT fields on all the diagrams apart from K/Y-Nb/Y, and melts derived from source regions with residual rutile explain high K/Y in **Figure 9a**. Similarly, **Figures 10a-g** show that the modelled melts derived from 'enriched' basaltic source regions with no residual rutile also easily intersect the ETT fields on all the diagrams apart from K/Y-Nb/Y and most of the ETT field in La/Y-Zr/Y. Partial melts derived from source regions with residual rutile can explain high K/Y in **Figure 10a**. These results suggest that partial melting of compositionally heterogeneous Eoarchaean arc-like mafic source regions with residual rutile can generate melts that explain most of the ETT geochemical variability.

5 A likely Eoarchaean geodynamic model

The mass balance models presented here suggest that the ETT can be generated by three main processes:

1. Partial melting, in the presence of slab-derived fluids, of relatively enriched, differentiated and altered non-arc metabasic source regions leaving a rutile-bearing residue. The melts ascend into the crust, lose their volatiles and crystallise as ETT.
2. A small proportion of ETT can still be generated by partial melting of primitive non-arc rutile-free metabasic source regions that mix with a slab-derived fluid. This is especially so if saline-rich slab fluids are involved.
3. Partial melting of variably altered metabasic crust that has island arc-like compositions. The melts ascend, lose any volatiles they may have and crystallise as ETT.

We argue that all three processes probably contributed to early Archaean continental growth, and that all require subduction zone processes. The models need to reproduce the ETT negative Nb-Ta anomaly on N-MORB normalised multielement diagrams as well as the enrichment in the incompatible elements. Our calculations show that for a non-arc metabasic protolith, ideally, both a slab fluid component and residual rutile are needed for generating ETT negative Nb-Ta anomalies (although a rutile free-source contaminated with a slab fluid can still explain some ETT compositions: Hastie et al. 2016a). However, experimental petrology demonstrates that residual rutile requires TiO_2 concentrations in the source region >1.0 wt.% (Klemme et al. 2002) and pressures of more than ~1.25-1.5 GPa (Patiño Douce and Beard 1995; Xiong et al., 2005) (>40-50 km). Eoarchaean mafic crust derived from 'normal' mantle melting can be up to 45 km thick, with many estimates being ~25 km (~0.8 GPa) (e.g., Hawkesworth et al. 2016, Kamber 2015). Therefore, it is doubtful whether intracrustal melting of non-arc metabasic crust derived by upper mantle melting or mantle plume activity can be a viable mechanism for ETT generation because of the lack of residual rutile at pressures less than ~1.25-1.5 GPa and the lack of a slab-fluid. Natural mafic granulites formed at similar depths to the estimates of Eoarchaean crustal thicknesses in a stagnant lid environment frequently contain ilmenite and magnetite, but lack rutile (Sheraton et al. 1980, Harley 1988, Ravindra Kumar and Chacko 1994, Hartel et al. 1996, Zhaoet al. 1999, Wu et al. 2012). Therefore, only intracrustal melting of Eoarchaean mafic crust with island arc-like compositions can form ETT magmas. This is also demonstrated in recent thermodynamic and geochemical studies of ETT(G) (Cox et al. 2018, Ge et al., 2018). However, to form mafic crust with arc-like affinities may require melting of a mantle source region to which a component ultimately derived from a deeper source region with residual rutile has been added (Pearce and Peate 1995, Jenner et al., 2009). In the absence of continental crust in the Eoarchaean and the lack of crustal assimilation in ETT (Hiess et al. 2009), the most plausible mechanism to form Eoarchaean mafic crust with arc affinities is by primitive subduction zones (possibly subcretion: Bédard 2013) (Jenner et al., 2009; Hoffmann et al., 2011).

It is possible that ETT could still be generated in a stagnant lid environment by inferring that the lower crust 'drips/delaminates' into the mantle. Crust penetrating deeper into the mantle may reach depths at which rutile is stabilised as a residual phase if the 'dripping' crust undergoes partial melting to form ETT melts. However, our modelling suggests that a slab fluid component is ideally required with residual rutile for generating the negative Nb-Ta anomalies and incompatible element enrichments in ETT from non-arc metabasic protoliths. Melts from a de-stabilised and foundering portion of lower non-arc Eoarchaean mafic crust would not mix with slab fluids, which are required to explain high LILE and LREE concentrations in ETT rock suites.

Although the Late Heavy Bombardment (LHB) is now controversial (e.g., Boehnke and Harrison 2016), geodynamic and geochemical models still propose that impacts linked to the LHB (Gomes et al. 2005) may be responsible for initiating subduction zone processes on the early Earth (O'Neill et al. 2017) and/or may be responsible for impact melting to form Hadean continental material (Johnson et al. 2018). Other geodynamic models also suggest that subduction processes (possibly short-lived), are viable in the Eoarchaean (e.g., Moyen and van Hunen, 2012; Sizova et al., 2015). Seismic and electrical anomalies below the Archaean Slave Craton, Canada have been linked to subduction at 3.5 Ga (Chen et al., 2009). Minerals trapped as inclusions in detrital Hadean zircons suggest that the zircons could be derived from melts at >4.0 Ga in ancient subduction zones (Hopkins et al. 2008). A recent statistical study of average basaltic geochemistry suggests that subduction and horizontal tectonics have operated consistently from the earliest Eoarchaean (Keller and Schoene 2018). Nutman and Friend (2009) also commented on the 'normality' of the rocks in the Eoarchaean record and emphasised that no lithologies are unique to the Eoarchaean era. They state that imbrication of volcanic and plutonic rocks with arc-like geochemical affinities by Eoarchaean accretion and collisional tectonics strongly suggests convergent margin processes.

While numerical modelling provides theoretical insights into the possible tectonic regimes on the early Earth we propose that a natural analogue for the solidification of the Earth's magma oceans can be found on lava lakes. Specifically, Duffield (1972) described a relatively large lava lake on Kilauea, Hawaii that developed all the basic elements of global plate tectonics. He showed that the surface of the lava lake solidified to form a thin crust that organised itself into crustal 'plates' that flowed laterally, driven by the convecting lava beneath. The boundaries of these 'plates' were fractures where new lava upwelled, amagmatic strike-slip occurred and where crustal plates underthrust each other. These three features resemble mid-ocean ridges, transform faults and subduction zones respectively. We suggest that as Hadean magma oceans solidified, the Earth's thin initial mafic surface crust was as dynamic as the crust on a lava lake; basically a thin crust on a restless magma layer. On a hot and thermomechanically active early Earth, it seems unlikely that the initial mafic lid was completely inert. We speculate that mid-oceanic ridges and zones of convergence developed very early on the Earth's surface. This is supported by Foley et al. (2014) who successfully modelled proto-subduction processes developing in the Hadean within ~100 Myrs of magma ocean solidification. We are not advocating modern-style plate tectonics on the early Earth, but instead suggest that primitive constructive and proto-convergent margins with shallow underthrusting developed. The formation of new crust, the lateral movement of early thin mafic plates and zones of convergence on the Hadean magma ocean was a type of early proto-plate tectonics that subsequently evolved into modern-day plate tectonics. This process would have led to hydrous melting and the formation of the ETT crust as soon as liquid water began to accumulate on the Earth's surface.

We propose that ETT magmas were generated in Eoarchaean subduction environments either by melting a subducting portion of thick and enriched (relative to N-MORB) non-arc metabasic crust and/or by intracrustal partial melting of island arc-like mafic crust. Additionally, Ge et al. (2018) suggest that Eoarchaean mafic arc material could subduct and melt to form ETT. We propose that plate tectonic-like processes began in the Hadean and formed the ETT. Although the style of plate tectonics would have been different on the early Earth it may be appropriate to consider plate tectonic style evolving over geological time as opposed to trying to define multiple styles of differing plate tectonic-like processes.

Acknowledgments

This work is made possible due to NERC Fellowship NE/J019372/1 awarded to A.R.H. We should like to thank Geoff Bromiley, Richard Brooker, David Cavell, Peter Cawood, Daniel

Cox, Jasmeet Dhaliwal, Wendell Duffield, James Kasting, Simon Harley, Chris Hawkesworth, Nic Odling, Tim Reston, Craig Storey and Sebastian Watt for helpful discussions over the years. We are particularly grateful for Wendell Duffield for sending us a DVD video of the Hawaiian lava lake where all the basic elements for global tectonics can be seen. Finally, we thank Claude Herzberg and an anonymous reviewer for helpful and constructive reviews.

References

Abbott, D., Drury, R., Smith, W.H.F., 1994. Flat to steep transition in subduction style. Geology 22, 937-940.

Adam, J., Rushmer, T., O'Neil, J., Francis, D., 2012. Hadean greenstones from the Nuvvuagittuq fold belt and the origin of the Earth's early continental crust. Geology 40, 363-366.

Baadsgaard, H., Nutman, A.P., Bridgewater, D., 1986. Geochronology and isotopic variation of the early Archaean Amitsoq gneisses of the Isukasia area, southern West Greenland. Geochimica et Cosmochimica Acta 50, 2173-2183.

Beard, J.S., Lofgren., G.E., 1991. Dehydration melting and water-saturated melting of basaltic and andesitic greenstones and amphibolites at 1, 3, and 6·9 kb. Journal of Petrology 32, 365-401.

Bédard, J.H., 2017. Stagnant lids and mantle overturns: Implications for Archaean tectonics, magmagenesis, crustal growth, mantle evolution, and the start of plate tectonics. Geoscience Frontiers. 9, 19-49.

Bédard, J.H., 2006). A catalytic delamination-driven model for coupled genesis of Archaean crust and sub-continental lithospheric mantle. Geochimica et Cosmochimica Acta 70, 1188-1214.

Bédard, J.H., Harris, L.B. & Thurston, P.C., 2013. The hunting of the snArc. Precambrian Research 229, 20-48.

Boehnke, P., Harrison, T.M., 2016. Illusory Late Heavy Bombardments. Proceedings of the National Academy of Sciences 113, 10,802-810,806.

Bowring, S. A., Williams, I.S., 1999. Priscoan (4.00-4.03 Ga) orthogneisses from northwestern Canada. Contributions to Mineralogy and Petrology 134, 3-16.

Castro, A., 2004. The source of granites: inferences from the Lewisian complex. Scottish Journal of Geology 40, 49-65.

Cawood, P. A., Hawkesworth, C.J., Dhuime, B., 2013. The continental record and the generation of continental crust. Geological Society of America Bulletin 125, 14-32.

Chen, C.-W., Rondenay, S., Evans, R.L., Snyder, D.B., 2009. Geophysical Detection of Relict Metasomatism from an Archaen (~3.5 Ga) Subduction zone. Science 326, 1089-1091.

Condie, K., 2005. TTGs and adakites: are they both slab melts? . Lithos 80, 33-44.

Cox, D., Kerr, A.C., Hastie, A.R., Kakarc, I., 2018. Petrogenesis of plagiogranites in the Muslim Bagh Ophiolite, Pakistan: implications for the generation of Archean continental crust. Geological Magazine, https://doi.org/10.1017/S0016756818000250.

Crowley, J. L., 2003. U-Pb geochronology of 3810-3630 Ma granitoid rocks south of the Isua greenstone belt, souther West Greenland. Precambrian Research 126, 235-257.

Davaille, A., Smrekar, S.E., Tomlinson, S., 2017. Experimental and observational evidence for plume-induced subduction on Venus. Nature Geoscience 10, 349-355.

Dhuime, B., Hawkesworth, C., Cawood, P., Storey, C.D., 2012. A change in the Geodynamics of Continental Growth 3 Billion Years Ago. Science 335, 1334-1336.

Dhuime, B., Wuestefeld, A., Hawkesworth, C.J., 2015. Emergence of modern continental crust about 3 billion years ago. Nature Geoscience 8, 552-555.

Drummond, M. S., Defant, M.J., Kepezhinskas, P.K., 1996. Petrogenesis of slab-derived trondjemite-tonalite-dacite/adakite magmas. Transactions of the Royal Society of Edinburgh: Earth Sciences 87, 205-215.

Duffield, W. A., 1972. A naturally occurring model of global plate tectonics. Journal of Geophyical Research 77, 2543-2555.

Elkins-Tanton, L.T., 2008. Linked magma ocean solidification and atmospheric growth for Earth and Mars. Earth and Planetary Science Letters 271, 181-191.

Ernst, W.G., Sleep, N.H., Tsujimori, T. 2016. Plate-tectonic evolution of the Earth: bottom-up and top-down mantle circulation. Canadian Journal of Earth Sciences 53, 1103-1120.

Fitton, J.G., Godard. M., 2004. Origin and evolution of magmas on the OJP. In: Fitton, J.G., Mahoney, J.J., Wallace, P.J., Saunders, A.D. (Eds) Origin and evolution of the OJP. Geological Society of London Special Publication 229, 151-178.

Foley, S.F., Tiepolo, M., Vannucci, R., 2002. Growth of early continental crust controlled by melting of amphibolite in subduction zones. Nature 417, 837-840.

Foley, B. J., Bercovici, D., Elkins-Tanton, L.T., 2014. Initiation of plate tectonics from post-magma ocean thermochemical convection. Journal of Geophyical Research 119, 8538-8561.

Francois, C., Philippot, P., Rey, P., Rubatto, D., 2014. Burial and exhumation during Archean sagduction in the East Pilbara Granite-Greenstone Terrane. Earth and Planetary Science Letters 396, 235-251.

Ge, R., Zhu, W., Wilde, S.A., Wu, H. 2018. Remnants of Eoarchean continental crust derived from a subducted proto-arc. Science Advances 4, 1-11.

Gomes, R., Levison, H.F., Tsiganis, K., Morbidelli, A., 2005. Origin of the cataclysmic Late Heavy Bombardment period of the terrestrial planets. Nature 435, 466-469.

Hamilton, W.B., 1998. Archean magmatism and deformation were not products of plate tectonics. Precambrian Research 91, 143-179.

Harley, S. L., 1988. Proterozoic Granulites from the Rauer Group, East Antarctica. I. Decompressional Pressure-Temperature Paths Deduced from Mafic and Felsic Gneisses. Journal of Petrology 29, 1059-1095.

Harley, S. L., Black, L.P., 1997. A revised Archaean chronology for the Napier Complex, Enderby Land, from SHRIMP ion-microprobe studies. Antarctic Science 9, 74-91.

Harrison, T. M., Blichert-Toft, J., Muller, W., Albarede, F., Holden, P., Mojzsis, S.J., 2005."Heterogeneous Hadean Hafnium: Evidence of continental crust at 4.4 to 4.5 Ga. Science 310, 1947-1950.

Hartel, T. H. D., Patterson, D.R.M ., 1996. Genesis of the Kapuskasing (Ontario) migmatitic mafic granulites by dehydration melting of amphibolite: the importance of quartz to reaction progress. Journal of Metamorphic Geology 14, 591-611.

Hastie, A.R., Fitton, J.G., Bromiley, G.D., Butler, I.B., Odling, N.W.A., 2016a. The origin of Earth's first continents and the onset of plate tectonics. Geology 44, 855-858.

Hastie, A.R., Fitton, J.G., Kerr, A.C., McDonald, I., Schwindrofska, A., Hoermle, K., 2016b. The composition of mantle plumes and the deep Earth. Earth and Planetary Science Letters 444, 13-25.

Hastie, A.R., Fitton, J.G., Mitchell, S.F., Neill, I., Nowell, G.M., Millar, I.L., 2015. Can fractional crystallization, mixing and assimilation processes be reponsible for Jamaican-type adakites? Implications for generating Eoarchaean continental crust. Journal of Petrology: doi: 10.1093/petrology/egv1029.

Hastie, A. R., Kerr, A. C., Pearce, J. A., Mitchell, S.F., 2007. Classification of altered island arc rocks using immobile trace elements: Development of the Th-Co discrimination diagram. Journal of Petrology 48, 2341-2357.

Hawkesworth, C. J., Cawood, P.A., Dhuime, B., Kemp, T.I.S., 2017. Earth's continental lithosphere through time. Annual Reviews of Earth and Planetary Science Letters 45, 169-198.

Hawkesworth, C. J., Cawood, P.A., Dhuime, B.,2016. Tectonics and crustal evolution. GSA 26, 4-11.

Hawkesworth, C. J., Kemp. A. I. S., 2006. Evolution of the continental crust. Nature 443, 811-817.

Herzberg, C., Condie, K., Korenaga, J., 2010. Thermal history of the Earth and its petrological expression. Earth and Planetary Science Letters 292, 79-88.

Herzberg, C., O'Hara, M.J., 2002. Plume-associated ultramafic magmas of Phanerozoic age. Journal of Petrology 43, 1857-1883.

Herzberg, C., Asimow, P.D., 2015. PRIMELT3 MEGA.XLSM software for primary magma calculation: Peridotite primary magma MgO contents from the liquidus to the solidus. Geochemistry Geophysics Geosystems 16, doi:10.1002/2014GC005631.

Hiess, J., Bennett, V.C., Nutman, A.P., Williams, I.S., 2009. In situ U-Pb, O and Hf isotope compositions of zircon and olivine from Eoarchaean rocks, West Greenland: New insights to making old crust. Geochimica et Cosmochimica Acta 73, 4489-4516.

Hoffmann, J. E., Nagel, T.J., Munker, C., Naeraa, T., Rosing, M.T., 2014. Constraining the process of Eoarchean TTG formation in the Itsaq Gneiss Complex, southern West Greenland. Earth and Planetary Science Letters 388, 374-386.

Hoffmann, J. E., Münker, C., Næraa, T., Rosing, M.T., Herwartz, D., Garbe-Schönberg, D., Svahnberg, H., 2011. Mechanisms of Archean crust formation inferred from high-precision HFSE systematics in TTGs. Geochimica et Cosmochimica Acta 75, 4157-4178.

Hopkins, M., Harrison, T.M., Manning, C.E., 2008. Low heat flow inferred from >4 Gyr zircons suggests Hadean plate boundary interactions. Nature 456, 493-496.

Iizuka, T., Komiya, T., Ueno, Y., Katayama, I., Uehara, Y., Maruyama, S., Hirata, T., Johnson, S.P., Dunkley, D.J., 2007. Geology and zircon geochronology of the Acasta Gneiss Complex, northwestern Canada: New constraints on its tectonothermal history. Precambrian Research 153, 179-208.

Jenner, F. E., Bennett, V.C., Nutman, A.P., Friend, C.R.L., Norman, M.D. , Yaxley, G., 2009. Evidence for subduction at 3.8 Ga: Geochemistry of arc-like metabasalts from the southern edge of the Isua Supracrustal Belt. Chemical Geology 261, 83-98.

Johnson, T. E., Brown, M., Gardiner, N.J., Kirkland, C.L., Smithies, H., 2017. Earth's first stable continents did not form by subduction. Nature 543, 239-242.

Johnson, T. E., Gardiner, N.J., Miljkovic., Spencer, C.J., Kirkland, C.L., Bland, P.A., Smithies, H., 2018. An impact melt origin for Earth's oldest known evolved rocks. Nature Geoscience 11, 795-799.

Kaczmarek, M.-A., Reddy, S.M., Nutman, A.P., Friend, C.R.L., Bennett, V.C., 2016. Earth's oldest mantle fabrics indicate Eoarchaean subduction. Nature Communications 7, 1-7.

Kamber, B. S. 2015. The evolving nature of terrestrial crust from the Hadean, through the Archaean, into the Proterozoic. Precambrian Research 258, 48-82.

Kamber, B. S., 2010. Archean mafic-ultramafic volcanic landmasses and their effect on ocean-atmosphere chemistry. Chemical Geology 274, 19-28.

Kamber, B. S., Whitehouse, M.J., Bolhar, R., Moorbath, S., 2005. Volcanic resurfacing and the early terrestrial crust: Zircon U-Pb and REE constraints from the Isua Greenstone Belt, southern West Greenland. Earth and Planetary Science Letters 240, 276-290.

Kamber, B. S., Ewart, A., Collerson, K.D., Bruce, M.C., McDonald, G.D., 2002. Fluid-mobile trace element constraints on the role of slab melting and implications for Archaean crustal growth models. Contributions to Mineralogy and Petrology 144, 38-56.

Keller, B. Schoene, B., 2018. Plate tectonics and continental basaltic geochemistry throughout Earth history. Earth and Planetary Science Letters 481, 290-304.
Kerr, A. C., 2014. Oceanic plateaus. In: Holland, H. and Turekian, K. eds. Treatise on geochemistry (2nd ed.) The crust. Amsterdam, Elsevier 4, 631-667.
Kerrich, R., Polat, A., 2006. Archean greenstone-tonalite duality: Thermochemical mantle convection models or plate tectonics in the early Earth global dynamics? Tectonophysics 415, 141-165.
Kinny, P. D., Nutman, A.P., 1996. Zirconology of the Meeberrie gneiss, Yilgarn Craton, Western Australia: an early Archaean migmatite. Precambrian Research 78, 165-178.
Klemme, S., Blundy, J.D., Wood, B.J., 2002. Experimental constraints on major and trace element partitioning during partial melting of ecologite. Geochimica et Cosmochimica Acta 66, 3109-3123.
Knauth, L. P., 2005. Temperature and salinity history of the Precambrian ocean: implications for the course of microbial evolution. Palaeontology Palaeoclimatology Palaeoecology 219, 53-69.
Kogiso, T., Tatsumi, Y., Nakano, S., 1997. Trace element transport during dehydration processes in the subducted oceanic crust: 1. Experiments and implications for the origin of ocean island basalts. Earth and Planetary Science Letters 148, 193-205.
Korenaga, J., Kelemen, P.B., 2000. Major element heterogeneity in the mantle source of the North Atlantic igneous province. Earth and Planetary Science Letters 184, 251-268.
Kusky, T. M., Windley, B.F., Safonova, I., Wakita, K., Wakabayashi, J., Polat, A., Santosh, M., 2013. Recognition of oceanic plate stratigraphy in accretionary orogens through Earth history: A record of 3.8 billion years of sea floor spreading, subduction, and accretion. Gondwana Research 24, 501-547.
Laurie, A., Stevens, G., 2012. Water-present eclogite melting to produce Earth's early felsic crust. Chemical Geology 317, 83-95.
Liu, D. Y., Wan, Y.S., Wu, J.S., Wilde, S.A., Zhou, H.Y., Dong, C.Y., Yin, X.Y., 2007. Eoarchean rocks and zircons in the North China Craton. Earth's Oldest Rocks. Van Kranendonk, M.J., Smithies, R.H. & Bennett, V.C. (eds). Developments in Precambrian Geology. 15, 251-273.
López, S., Castro, A., 2000. Determination of the fluid-absent solidus and supersolidus phase relationships of MORB-derived amphibolites in the range 4-14 kbar. American Mineralogist 86, 1396-1403.
Macpherson, C. G., Dreher, S.T., Thirlwall, M.F., 2006. Adakites without slab melting: High pressure differentiation of island arc magma, Mindanao, the Philippines. Earth and Planetary Science Letters 243, 581-593.
Martin, H., Smithies, R.H., Rapp, R., Moyen, J-F., Champion, D., 2005. An overview of adakite, tonalite-trondhjemite-granodiorite (TTG), and sanukitoid: relationships and some implications for crustal evolution. Lithos 79, 1-24.
Martin, H., Moyen, J-F., 2002. Secular changes in tonalite-trondhjemite-granodiorite composition as markers of the progressive cooling of Earth. Geology 30, 319-322.
McDonough, W. F., Sun, S.-s., 1995. The composition of the Earth. Chemical Geology 120, 223-253.
Moore, W. B., Webb, A.A.G., 2013. Heat-Pipe Earth. Nature 501, 501-505.
Moyen, J-F., Laurent, O., 2018. Archaean tectonic systems: A view from igenous rocks. Lithos 302-303, 99-125.
Moyen, J-F., Martin, H., 2012. Forty years of TTG research. Lithos 148, 312-336.
Moyen, J-F., van Hunen, J., 2012. Short-term episodicity of Archaean plate tectonics. Geology 40, 451-454.

Moyen, J-F., Stevens, G., 2006. Experimental Constraints on TTG Petrogenesis: Implications for Archean Geodynamics: Archean Geodynamics and Environments. American Geophysical Union Geophysical Monograph Series 164, 149-175.

Nagel, T. J., Hoffmann, J.E., Münker, C. 2012. Generation of Eoarchean tonalite-trondhjemite-granodiorite series from thickened mafic arc crust. Geology 40, 375-378.

Nebel, O., Campbell, I.H., Sossi, P.A., Van Kranendonk, M.J., 2014. Hafnium and iron isotopes in early Archean komatiites record a plume-driven convection cycle in the Hadean Earth. Earth and Planetary Science Letters 397, 111-120.

Nutman, A. P., Bennett, V.C., Friend, C.R.L., 2015. The emergence of the Eoarchaean proto-arc: evolution of a c. 3700 Ma convergent plate boundary at Isua, southern West Greenland. Geological Society of London Special Publication 389, 113-133.

Nutman, A. P., Bennett, V.C., Friend, C.R.L., Jenner, F., Wan, Y., Liu, D. 2009. Eoarchaean crustal growth in West Greenland (Itsaq Gneiss Complex) and in northeastern China (Anshan area): review and synthesis. In: Cawood, P.A., Kröner, A., (Eds.), Earth Accretionary Systems in Space and Time, Geological Society of London, Special Publication 318, 127-154.

Nutman, A. P. Friend, C.R.L., 2009. New 1:20,000 scale geological maps, synthesis and history of investigation of the Isua supracrustal belt and adjacent orthogneisses, southern West Greenland: A glimpse of Eorchaean crust formation and orogeny. Precambrian Research 172, 189-211.

Nutman, A. P., Bennett, V.C., Friend, C.R.L., Horie, K., Hidaka, H., 2007. ~3,850 Ma tonalites in the Nuuk region, Greenland: geochemistry and their reworking within an Eoarchaean gneiss complex. Contributions to Mineralogy and Petrology 154, 385-408.

Nutman, A. P., Bennett, V.C., Friend, C.R.L., Norman, M., 1999. Meta-igneous (non-gneissic) tonalites and quartz-diorites from an extensive ca. 3800 Ma terrain south of the Isua supracrustal belt, southern West Greenland: Constraints on early crust formation. Contributions to Mineralogy and Petrology 137, 364-388.

Nutman, A. P., Bennett, V.C., Kinny, P.D., Price, R., 1993. Large-scale crustal structure of the northwestern Yilgarn Craton, Western Australia: Evidence from Nd isotopic data and zircon geochronology. Tectonics 12, 971-981.

Nutman, A. P., Bridgewater, D., 1986. Early Archaean Amitsoq tonalites and granites of the Isukasia area, southern West Greenland: develpment of the oldest-known sial. Contributions to Mineralogy and Petrology 94, 137-148.

O'Neil, J., Carlson, R.W., 2017. Building Archean cratons from Hadean mafic crust. Science 355, 1199-1202.

O'Neil, J., Rizo, H., Boyet, M., Carlson, R.W., Rosing, M.T., 2016. Geochemistry and Nd isotopic characteristics of Earth's Hadean mantle and primitive crust. Earth and Planetary Science Letters 442, 194-205.

O'Neil, J., Maurice, C., Stevenson, R.K., Larocque, J., Cloquet, C., David, J., Francis, D., 2007. The geology of the 3.8 Ga Nuvvuagittuq (Porpoise Cove) greenstone belt, northeastern Superior Province, Canada. Earth's Oldest Rocks. Van Kranendonk, M.J., Smithies, R.H. & Bennett, V.C. (eds). Developments in Precambrian Geology. 15, 219-250.

O'Neill, C. O., Marchi, S., Zhang, S., Bottke, W., 2017. Impact-driven subduction on the Hadean Earth. Nature Geoscience 10, 793-797.

Palin, R. M., White, R.W., Green, E., 2016a. Partial melting of metabasic rocks and the generation of tonalitic-trondhjemitic-granodioritic (TTG) crust in the Archaean: Constraints from phase equilibrium modelling. Precambrian Research 287, 73-90.

Palin, R. M., White, R.W., 2016b. Emergence of blueschists on Earth linked to secular changes in oceanic crust composition. Nature Geoscience 9, 60-64.

Patiño Douce, A. E., Beard, J.S., 1995. Dehydration-melting of biotite gneiss and quartz amphibolite from 3 to 15 kbar. Journal of Petrology 36, 707-738.

Peacock, S. M., Rushmer, T., Thompson, A.B., 1994. Partial melting of subducting oceanic crust. Earth and Planetary Science Letters 121, 227-244.

Pearce, J. A., Peate, D. W., 1995. Tectonic implications of the composition of volcanic arc magmas. Annual Reviews of Earth and Planetary Science Letters 23, 251-285.

Polat, A., Wang, L., Appel, P.W.U., 2015. A review of structural patterns and melting processes in the Archean craton of West Greenland: Evidence for crustal growth at convergent plate margins as opposed to non-uniformitarian models. Tectonophysics 662, 67-94.

Polat, A., Hofmann, A.W., 2003. Alteration and geochemical patterns in the 3.7-3.8 Ga Isua greenstone belt, West Greenland. Precambrian Research 126, 197-218.

Rapp, R. P., Shimizu, N., Norman, M.D., 2003. Growth of early continental crust by partial melting of eclogite. Nature 425, 605-608.

Rapp, R. P., Shimizu, N., Norman, M.D., Applegate, G.S., 1999. Reaction between slab-derived melts and peridotite in the mantle wedge: experimental constraints at 3.8 GPa. Chemical Geology 160, 335-356.

Rapp, R. P., Watson, E.B., 1995. Dehydration melting of metabasalt at 8-32 kbar: implications for continental growth and crust-mantle recycling. Journal of Petrology 36, 891-931.

Ravindra Kumar, G. R., Chako, T., 1994. Geothermobarometry of mafic granulites and metapelite from the Palghat Gap, South India: petrological evidence for isothermal uplift and rapid cooling. Journal of Metamorphic Geology 12, 479-492.

Reimink, J. R., Chacko, T., Stern, R.A., Heaman, L.M., 2014. Earth's earliest evolved crust generated in an Iceland-like setting. Nature Geoscience 7, 529-533.

Robin, C. M. I., Bailey, R.C., 2009. Simultaneous generation of Archean crust and subcratonic roots by vertical tectonics. Geology 37, 523-526.

Rozel, A. B., Golabek, G.J., Jain, C., Tackley, P.J., Gerya, T., 2017. Continental crust formation on early Earth controlled by intrusive magmatism. Nature 545, 332-335.

Rushmer, T., 1991. Partial melting of two amphibolites: contrasting experimental results under fluid-absent conditions. Contributions to Mineralogy and Petrology 107, 41-59.

Sautter, V., Toplis, M.J., Wiens, R.C., Cousin, A., Fabre, C., Gasnault, O., Maurice, S., Forni, O., Lasue, J., Ollila, A., Bridges, J.C., Mangold, N., Le Mouelic, S., Fisk, M., Meslin, P.-Y., Beck, P., Pinet, P., Le Deit, L., Rapin, W., Stolper, E.M., Newsom, H., Dyar, D., Lanza, N., Vaniman, D., Clegg, S., Wray, J.J. 2015. In situ evidence for continental crust on early Mars. Nature Geoscience 8, 605-609.

Sen, C., Dunn, T., 1994. Dehydration melting of a basaltic composition amphibolite at 1.5 and 2.0 GPa: implications for the origin of adakites. Contributions to Mineralogy and Petrology 117, 394-409.

Sizova, E., Gerya, T., Stuwe, K., Brown, M., 2015. Generation of felsic crust in the Archean: A geodynamic modeling perspective. Precambrian Research 271, 198-224.

Shaw, D. M., 1970. Trace element fractionation during anatexis. Geochimica et Cosmochimica Acta 34, 237-243.

Sheraton, J. W., Offe, L.A., Tingey, R.J., Ellis, D.J., 1980. Enderby Land, Antarctica - an unusual Precambrian high-grade metamorphic terrain. Journal of the Geological Society of Australia 27, 1-18.

Shirey, S. B., Kamber, B.S., Whitehouse, M.J., Mueller, P.A., Basu, A.R., 2008. A review of the isotopic and trace element evidence for mantle and crustal processes in the Hadean and Archean: Implications for the onset of plate tectonic subduction. The Geological Society of America Special Paper 440, 1-29.

Skjerlie, K. P., Patino Douce, A.E., 1995. Anatexis of interlayered amphibolite and pelite at 10 kbar: effect of diffusion of major components on phase relations and melt fraction. Contributions to Mineralogy and Petrology 122, 62-78.

Skjerlie, K. P., Pation Douce, A.E., 2002. The fluid-absent partial melting of a zoisite-bearing quartz eclogite from 1.0 to 3.2 GPa; implications for melting in thickened continental crust and for subduction-zone processes. Journal of Petrology 43, 291-314.

Smithies, R. H., Champion, D.C., Cassidy, K.F., 2003. Formation of Earth's early Archaean continental crust. Precambrian Research 127, 89-101.

Smithies, R. H., Champion, D.C., Van Kranendonk, M.J., 2009. Formation of Paleoarchean continental crust through infracrustal melting of enriched basalt. Earth and Planetary Science Letters 281, 298-306.

Springer, W., Seck, H.A., 1997. Partial fusion of basic granulites at 5 to 15 kbar: implications for the origin of TTG magmas. Contributions to Mineralogy and Petrology 127, 30-45.

Steenfelt, A., Garde, A.A., Moyen, J-F., 2005. Mantle wedge involvement in the petrogenesis of Archaean grey gneisses in West Greenland. Lithos 79, 207-228.

Stern, R. J., Leybourne, M.I., Tsujimori, T., 2016. Kimberlites and the start of plate tectonics. Geology 44, 799-802.

Sun, S.-s., McDonough, W.F., 1989. Chemical and isotope systematics of oceanic basalts: implications for mantle composition and processes. Magmatism in the Ocean Basins. Geological Society of London Special Publication 42, 313-345.

Tang, M., Chen, K., Rudnick, R.L., 2016. Archean upper crust transition from mafic to felsic marks the onset of plate tectonics. Science 351, 372-375.

Tatsumi, Y., Kogiso, T., 1997. Trace element transport during dehydration processes in the subducted oceanic crust: 2. Origin of chemical and physical characteristics in arc magmatism. Earth and Planetary Science Letters 148, 207-221.

Thebaud, N., Ray, P.F., 2013. Archean gravity-driven tectonics on hot and flooded continents: Controls on long-lived mineralised hydrothermal systems away from continental margins. Precambrian Research 229, 93-104.

Van Hunen, J., Moyen, J-F., 2012. Archean Subduction: Fact or Fiction? . Annual Reviews of Earth and Planetary Sciences 40, 195-219.

Van Thienen, P., van den Berg, A.P., Vlaar, N.J., 2004. On the formation of continental silicic melts in thermochemical mantle convection models: implications for early Earth. Tectonophysics 394, 111-124.

Walter, M. J., 1998. Melting of Garnet Peridotite and the Origin of Komatiite and Depleted Lithosphere. Journal of Petrology 39, 29-60.

Wiemer, D., Schrank, C.E., Murphy, D.T., Wenham, L., Allen, C.M., 2018. Earth's oldest stable crust in the Pilbara Craton formed by cyclic gravitatinal overturns. Nature Geoscience 11, 357-361.

Winther, K. T., 1996. An experimentally based model for the origin of tonalitic and trondhjemitic melts. Chemical Geology 127, 43-59.

Wolf, M. B., Wyllie, P.J., 1994. Dehydration-melting of amphibolite at 10 kbar: the effects of temperature and time. Contributions to Mineralogy and Petrology 115, 369-383.

Wu, M., Zhao, G., Sun, M., Yin, C., Li, S., Tam, P.Y., 2012. Petrology and P-T path of the Yishui mafic granulites: Implications for tectonothermal evolution of the Western Shandong Complex in the Eastern Block of the North China Craton. Precambrian Research 222-223, 312-324.

Xiong, X. L., Adam, J., Green, T.H., 2005. Rutile stability and rutile/melt HFSE partitioning during partial melting of hydrous basalt: Implications for TTG genesis. Chemical Geology 218, 339-359.

Zhang, C., Holtz, F., Koepke, J., Wolff, P.E., Ma, C., Bédard, J.H., 2013. Contraints from experimental melting of amphibolite on the depth of formation of garnet-rich restites, and implications for models of Early Archean crustal growth. Precambrian Research 231, 206-217.

Zhao, G., Wilde, S.A., Cawood, P.A., Lu, L., 1999. Thermal evolution of two textural types of mafic granulites in the North China craton: evidence for both mantle plume and collisional tectonics. Geological Magazine 136, 223-240.

Ziaja, K., Foley, S.F., White, R.W., Buhre, S., 2014. Metamorphism and melting of picritic crust in the early Earth. Lithos 189, 173-184. .

Figure Captions

Fig 1: Simple cartoons to show the tectonic models used to explain the generation of ETT plutons. **Model 1:** upwelling hot Eoarchaean mantle leads to the formation of ETT magmas due to partial melting of the base of existing thick probably mafic crust. Additionally, a crustal 'drip' could undergo partial fusion to generate ETT magmas. **Model 2:** a ~45 km thick oceanic plateau-like slab subducts beneath another at a flat/shallow angle. The slab shear surface undergoes fusion to form large volumes of ETT magmas.

Fig 2: Various classification diagrams modified from Moyen and Martin (2012) and Martin et al. (2005). **(a)** an Anorthite-Albite-Orthoclase classification diagram. **(b)** A (La/Yb)cn-(Yb)cn (chondrite normalised) diagram highlighting the compositional difference between young granites and Archaean TTG. **(c)** A Sr-Na_2O+CaO diagram highlighting the geochemical difference between young TTG and ETT. ETT data from Kamber et al. (2002) Hoffmann et al. (2011; 2014), Nutman et al. (2009) and Ge et al. (2018).

Fig 3: N-MORB-normalised multielement diagrams showing **(a)** analysed trace element concentrations of tonalite-composition glasses in OJP-derived partial melt experiments reported by Hastie et al. (2016a) (sample designations indicate if plagioclase and/or garnet was stable along with amphibole). **(b)** Modelled tonalite + slab fluid mixtures from Hastie et al. (2016a). **(c)** Theoretical compositions of the partial melts in OJP partial melt experiments from Hastie et al. (2016a) calculated using the mass balance technique outlined in this paper (see Tables 1-4). ETT data from Kamber et al. (2002) Hoffmann et al. (2011; 2014), Nutman et al. (2009) and Ge et al. (2018).

Fig 4: Representative incompatible trace element ratio diagrams showing calculated partial melt compositions for metabasic source regions with an N-MORB starting composition from Hofmann (1988). Note that the TiO_2 concentration from Hofmann has been increased from 1.615 to 2.0 wt.%. Yellow circles are calculated melts from rutile-free source regions and green circles are from liquids calculated from rutile-bearing protoliths. Figure 4b is the same as Figure 4a except that batch melt compositions are compared to melt compositions calculated by using Shaw's (1970) accumulated fractional melting equation, as described in section 3.1 (also see 4f and 4g). All other diagrams show batch-melt compositions. ETT field constructed from data in Kamber et al. (2002) Hoffmann et al. (2011; 2014), Nutman et al.

(2009) and Ge et al. (2018); Island arc field from data in Pearce et al. (1995) and Elliott et al. (1997); MORB data from Dosso et al. (1993), Regelous et al. (1999) and Wendt et al. (1999); Ocean Island Basalt (OIB) data from Salters et al. (2010), Workman et al. (2004) and Woodhead et al. (1996); Oceanic Plateau data from Fitton and Godard (2004) and Hastie et al. (2016b). Experimentally derived liquids from MORB starting composition are from Laurie and Stevens (2012).

Fig 5: Representative incompatible trace element ratio diagrams showing calculated partial melt compositions for metabasic source regions with an OJP starting composition; sample 1187-8 from Fitton and Godard (2004). Yellow circles are calculated melts from rutile-free source regions and green circles are from liquids calculated from rutile-bearing protoliths. Fields constructed as in Figure 4. Experimentally derived liquids from OJP starting composition and OJP melt and slab fluid mixtures are from Hastie et al. (2016a) and Tables 1-4 respectively.

Fig 6: (a) N-MORB-normalised multielement diagram showing a larger range of elements than were reported by Hastie et al. (2016a) in calculated OJP-derived tonalite + slab fluid mixtures (Tables 1-4). (b-j) Major element variation diagrams showing ETT data from Kamber et al. (2002) Hoffmann et al. (2011; 2014), Nutman et al. (2009) and Ge et al. (2018) relative to our newly calculated OJP-derived tonalite + slab fluid mixtures (Tables 1-4).

Fig 7: Representative incompatible trace element ratio diagrams showing calculated partial melt compositions for **(1)** a metabasic source region with a theoretical Eoarchaean crustal composition after 20% fractionation of a cotectic assemblage (light blue circles); **(2)** the same source region as (1), but with 10% fractional crystallisation of a low pressure mineral assemblage (plagioclase: 0.743, amphibole: 0.215, magnetite: 0.042), a high pressure mineral assemblage (amphibole: 0.1745, clinopyroxene: 0.5296, orthopyroxene: 0.1725, garnet: 0.1234) and amphibole only (dark blue, dark red and light green circles respectively); **(3)** partial melting the source region in (1) that has undergone 20% hydrothermal alteration (dark green circles). Fields constructed as in Figure 4.

Fig 8: Representative incompatible trace element ratio diagrams showing calculated partial melt compositions for **(1)** a metabasic source region with a theoretical Eoarchaean crustal composition after 50% fractionation of a cotectic assemblage (light blue circles); **(2)** the same source region as (1), but with 10% fractional crystallisation of a low pressure mineral assemblage (plagioclase: 0.743, amphibole: 0.215, magnetite: 0.042), a high pressure mineral assemblage (amphibole: 0.1745, clinopyroxene: 0.5296, orthopyroxene: 0.1725, garnet: 0.1234) and amphibole only (dark blue, dark red and light green circles respectively); **(3)** partial melting the source region in (1) that has undergone 20% hydrothermal alteration (dark green circles). Fields constructed as in Figure 4.

Fig 9: Representative incompatible trace element ratio diagrams showing calculated partial melt compositions for a metabasic source region with an average ‘normal’ Eoarchaean metabasic amphibolite, with island arc-like compositions (Jenner et al. 2009). Yellow circles are calculated melts from rutile-free source regions and green circles are from liquids

calculated from rutile-bearing protoliths. Fields constructed as in Figure 4. Experimentally derived liquids from greenstone and back-arc starting compositions are from Adam et al. (2012) and Rapp et al. (1999) respectively.

Fig 10: Representative incompatible trace element ratio diagrams showing calculated partial melt compositions for a metabasic source region with an average 'enriched' Eoarchaean metabasic amphibolite, with island arc-like compositions (Jenner et al. 2009). Yellow circles are calculated melts from rutile-free source regions and green circles are from liquids calculated from rutile-bearing protoliths. Fields constructed as in Figure 4. Experimentally derived liquids from greenstone and back-arc starting compositions are from Adam et al. (2012) and Rapp et al. (1999) respectively.

OJP tonalite partial melts	Temperature (°C)	Pressure (GPa)	Water added (wt.%)	SiO_2	TiO_2	Al_2O_3	FeO(t)	MnO	MgO	CaO	Na_2O	K_2O	P_2O_5	Total
OJPgwe1	925	2.0	2.2	68.82	0.37	17.08	2.81	0.05	1.36	5.12	3.72	0.45	0.23	100
OJPgw13	950	1.8	2.2	66.64	0.47	18.01	3.63	0.07	1.59	5.70	3.26	0.36	0.26	100
OJPgw11	950	1.6	1.8	68.80	0.22	17.03	2.74	0.07	1.47	4.87	3.92	0.53	0.35	100
OJPgw3	925	1.6	2.5	67.70	0.27	17.64	2.51	0.08	1.83	5.64	3.69	0.38	0.28	100
OJPgw24	950	2.2	2.1	70.32	0.55	16.42	2.49	0.03	1.40	4.50	3.60	0.48	0.20	100
OJPgw9	900	2.0	2.1	70.27	0.25	16.61	2.35	0.06	1.30	5.04	3.22	0.57	0.33	100
OJPgw5	900	1.8	2.3	72.26	0.15	16.17	1.44	0.06	1.18	4.45	3.74	0.56	-	100
OJPgw6	925	1.8	2.7	71.62	0.18	15.75	1.74	0.07	1.48	5.46	3.23	0.47	-	100
OJPgw8	925	2.0	3.1	69.80	0.49	17.11	2.46	0.03	1.28	4.94	3.52	0.37	-	100
OJPgw10	925	2.0	2.2	67.50	0.54	16.56	3.58	0.04	2.35	5.46	3.43	0.38	0.15	100

Table 1 – Experimental conditions and average tonalite major element melt compositions derived from hydrous OJP-derived partial melt experiments in Hastie et al (2016a). Melt compositions are re-calculated to 100% totals, minus chlorine and sulphur analyses, so they can be compared to ETT compositions in the literature. All elements are derived from electron microprobe apart from TiO_2 data that are from ion microprobe and LA-ICP-MS analysis (used so it is compatible with trace element modelling).

OJP tonalite partial melts	SiO_2	TiO_2	Al_2O_3	FeO(t)	MnO	MgO	CaO	Na_2O	K_2O	P_2O_5	Total	Ba	Th	U	Nb	Ta	La	Ce	Sr	Pr	Nd	Zr	Ti	Gd	Tb	Dy	Y	Ho	Yb	Lu
OJPgwe1	62.06	0.36	15.91	5.96	0.05	2.47	6.40	4.01	4.11	2.15	99.61	61.70	8.17	4.00	5.66	4.08	1.77	19.51	69.82	3.98	3.87	76.00	4.60	9.04	1.47	8.11	8.44	1.46	4.40	1.40
OJPgw13	60.00	0.00	16.51	3.82	0.07	1.76	5.29	2.99	0.33	0.23	91.01	70.00	9.05	4.95	5.41	4.88	8.88	20.43	40.49	5.97	7.19	95.81	7.55	4.43	3.33	7.77	7.73	3.44	0.00	0.00
OJPgw11	63.00	0.00	15.52	2.07	0.06	1.76	4.39	3.01	0.00	0.00	92.01	99.00	14.45	5.07	7.76	5.21	6.13	31.00	33.20	2.29	8.92	20.02	2.97	9.71	1.96	8.40	9.16	1.80	6.80	0.00
OJPgw3	61.00	0.00	16.51	2.09	0.07	1.76	5.35	3.01	0.00	0.00	91.01	11.00	6.30	3.00	6.01	2.81	1.16	16.01	88.67	2.78	7.18	75.27	3.30	1.01	1.15	5.42	4.35	2.02	0.00	0.00
OJPgw24	60.00	0.00	16.51	2.08	0.07	1.76	5.29	2.99	0.00	0.00	91.01	75.00	8.67	3.70	6.01	5.09	1.05	22.01	24.47	3.09	3.31	38.83	3.33	9.98	1.86	6.62	6.99	2.09	0.00	0.00
OJPgw9	61.00	0.00	16.51	2.08	0.07	1.76	5.29	2.99	0.00	0.00	91.01	11.00	8.44	4.00	4.58	7.85	7.85	16.51	74.49	7.94	8.49	99.98	2.27	7.77	2.82	9.93	9.96	7.78	5.25	2.45
OJPgw5	56.00	0.00	16.51	2.08	0.07	1.76	5.29	2.99	0.00	0.00	91.01	-	-	-	-	-	-	-	-	-	-	-	-	-	-	-	-	-	-	-
OJPgw6	66.00	0.00	16.51	2.08	0.07	1.76	5.29	2.99	0.00	0.00	91.01	-	-	-	-	-	-	-	-	-	-	-	-	-	-	-	-	-	-	-
OJPgw8	63.00	0.00	16.51	2.08	0.07	1.76	5.29	2.99	0.00	0.00	91.01	-	-	-	-	-	-	-	-	-	-	-	-	-	-	-	-	-	-	-
OJPgw10	79.00	0.00	12.51	2.08	0.07	1.76	5.29	2.99	0.00	0.00	91.01	-	-	-	-	-	-	-	-	-	-	-	-	-	-	-	-	-	-	-

Table 2 – Average tonalite major and trace element melt compositions derived from hydrous OJP-derived partial melt experiments in Hastie et al (2016a). Melt compositions are 'wet' analyses not re-calculated to 100%, but chlorine and sulphur analyses have been removed. All elements are derived from electron microprobe apart from TiO_2 data that are from ion microprobe and LA-ICP-MS analysis (used so it is compatible with trace element modelling).

	SiO_2	TiO_2	Al_2O_3	FeO(t)	MnO	MgO	CaO	Na_2O	K_2O	P_2O_5	H_2O	Ba	Th	U	Nb	Ta	La	Ce	Sr	Pr	Nd	Zr	Ti	Gd	Tb	Dy	Y	Ho	Yb	Lu
Anhydrous OJP																														
Kroenke	49.93	0.75	15.36	9.88	0.18	9.27	12.71	1.72	0.14	0.06	0.00	8.77	0.16	0.05	2.32	0.14	2.02	5.54	82	0.87	4.65	40.8	447.6	2.19	0.40	2.81	17.71	0.63	1.75	0.29
Kwaimbaita	50.85	1.19	14.52	11.18	0.20	7.53	12.04	2.21	0.17	0.10	0.00	13.28	0.28	0.10	3.51	0.22	3.34	9.22	109	1.43	7.59	64.9	712.3	3.48	0.62	4.32	24.90	0.92	2.41	0.39
Singgalo	49.91	1.61	14.52	12.08	0.22	6.89	12.12	2.38	0.13	0.14	0.00	24.11	0.53	0.13	6.50	0.38	5.55	15.17	166	2.21	10.93	104.1	968.2	4.54	0.75	5.21	30.83	1.06	2.43	0.41
Volcaniclastic	60.06	1.78	13.13	10.39	0.05	4.56	1.56	1.34	7.08	0.05	0.00	10.41	0.44	0.42	5.07	0.35	4.70	10.73	140	1.70	8.73	93.9	1066.9	3.29	0.56	3.70	15.34	0.72	1.67	0.25
HNB	50.92	1.47	16.69	12.11	0.23	5.57	7.47	4.81	0.53	0.20	0.00	32.91	0.77	0.24	8.82	0.52	7.79	17.92	145	2.47	12.55	100.3	8804	4.98	0.96	6.27	42.57	1.47	4.34	0.72
Hydrous OJP																														
Kroenke	49.43	0.74	15.20	9.78	0.18	9.18	12.58	1.70	0.14	0.06	1.00	8.69	0.16	0.05	2.29	0.14	2.00	5.49	82	0.86	4.60	40.4	443.2	2.16	0.40	2.78	17.54	0.62	1.73	0.29
Kwaimbaita	50.35	1.18	14.38	11.06	0.20	7.45	11.92	2.19	0.17	0.10	1.00	13.15	0.28	0.10	3.48	0.22	3.30	9.12	108	1.41	7.51	64.3	705.2	3.44	0.61	4.28	24.65	0.91	2.39	0.39
Singgalo	49.41	1.60	14.37	11.96	0.22	6.82	12.00	2.35	0.13	0.14	1.00	23.87	0.53	0.13	6.43	0.38	5.49	15.01	164	2.19	10.82	103.0	9585	4.50	0.74	5.16	30.52	1.05	2.41	0.41
Volcaniclastic	59.46	1.76	13.00	10.28	0.05	4.51	1.54	1.33	7.01	0.05	1.00	10.31	0.43	0.42	5.02	0.35	4.65	10.62	138	1.69	8.65	93.0	1056.2	3.25	0.56	3.66	15.19	0.71	1.65	0.25
HNB	50.41	1.45	16.52	11.99	0.23	5.51	7.40	4.76	0.52	0.20	1.00	32.58	0.76	0.23	8.74	0.52	7.71	17.74	143	2.45	12.43	99.3	8716	4.93	0.95	6.21	42.14	1.46	4.30	0.71
Average protolith	49.98	1.19	14.63	10.93	0.19	7.71	11.85	2.09	0.32	0.10	1.00	15.28	0.33	0.10	4.14	0.25	3.66	9.97	119	1.50	7.72	70.1	7128	3.38	0.59	4.08	24.19	0.86	2.18	0.36
Element mobility factor																														

| | | |

	SiO_2	TiO_2	Al_2O_3	FeO(t)	MnO	MgO	CaO	Na_2O	K_2O	P_2O_5	Total	Ba	Th	U	Nb	Ta	La	Ce	Sr	Pr	Nd	Zr	Ti	Gd	Tb	Dy	Y	Ho	Yb	Lu
OJP-derived tonalite + slab flux mix (96:4 ratio) on the slab shear surface																														
OJPgwe1	60.29	0.32	14.96	2.46	0.04	1.19	4.48	4.40	1.20	0.20	89.55	90.94	1.33	0.51	7.25	0.46	14.15	33.62	452.32	3.87	14.70	55.29	1670.40	0.91	0.16	0.78	4.64	0.15	0.42	0.10
OJPgw13	58.55	0.41	15.82	3.19	0.06	1.40	5.01	4.00	1.12	0.22	89.80	99.08	1.35	0.56	7.81	0.55	14.73	35.04	389.94	4.07	16.90	78.65	2280.22	2.06	0.22	1.85	7.46	0.36	0.80	0.23
OJPgw11	60.85	0.19	15.07	2.42	0.06	1.30	4.31	4.60	1.28	0.31	90.40	127.41	1.59	0.55	6.69	0.55	16.15	39.55	321.06	4.20	19.04	85.63	1170.78	1.65	0.19	1.32	9.11	0.34	1.04	0.19
OJPgw3	59.37	0.24	15.47	2.20	0.07	1.60	4.95	4.37	1.14	0.24	89.65	141.13	1.13	0.41	5.81	0.27	15.04	33.81	373.99	4.23	17.67	88.10	1415.68	1.65	0.26	2.33	9.89	0.49	1.36	0.24
OJPgw24	59.80	0.47	13.96	2.12	0.02	1.19	3.82	4.20	1.22	0.17	86.98	103.70	1.33	0.48	10.66	0.76	16.38	37.14	552.75	4.53	17.15	65.57	2013.82	0.42	0.12	1.41	2.59	0.08	0.25	0.02
OJPgw9	59.46	0.21	14.05	1.99	0.05	1.10	4.27	3.86	1.29	0.28	86.56	141.44	1.30	0.50	6.19	0.84	23.37	48.69	648.78	6.18	21.87	127.58	1314.24	3.05	0.31	0.89	8.61	0.64	0.55	0.24
OJPgw5	63.31	0.13	14.17	1.26	0.06	1.03	3.90	4.42	1.30		89.56																			
OJPgw6	62.84	0.16	13.82	1.52	0.06	1.30	4.80	3.97	1.22		89.69																			
OJPgw8	58.17	0.41	14.26	2.05	0.03	1.07	4.12	4.07	1.12		85.29																			
OJPgw10	58.36	0.47	14.32	3.10	0.03	2.03	4.72	4.10	1.14	0.13	88.40																			
OJP-derived tonalite + slab flux mix (96:4 ratio) after degassing and ascent into the crust																														
OJPgw	**67.3**	**0.36**	**16.7**	**2.75**	**0.05**	**1.33**	**5.01**	**4.91**	**1.34**	**0.22**	**100**	**101.5**	**1.49**	**0.57**	**8.10**	**0.52**	**15.8**	**37.5**	**505.1**	**4.32**	**16.4**	**61.74**	**1865.3**	**1.01**	**0.18**	**0.87**	**5.19**	**0.17**	**0.47**	**0.11**

e1	3		1								5				0	4	1		1		3															
OJPgw13	65.20	0.46	17.62	3.55	0.07	1.56	5.58	4.46	1.25	0.25	100	110.34	1.51	0.62	8.70	0.62	16.40	39.02	434.25	4.53	18.82	87.59	2539.35	2.29	0.25	2.07	8.31	0.40	0.89	0.25
OJPgw11	67.32	0.21	16.67	2.68	0.07	1.44	4.77	5.09	1.41	0.34	100	140.95	1.76	0.61	7.40	0.60	17.87	43.75	355.16	4.65	21.06	94.72	1295.15	1.82	0.21	1.46	10.08	0.38	1.15	0.21
OJPgw3	66.23	0.26	17.26	2.45	0.07	1.79	5.52	4.88	1.27	0.27	100	157.43	1.27	0.45	6.48	0.30	16.78	37.72	417.19	4.72	19.71	98.28	1579.19	1.84	0.29	2.60	11.03	0.55	1.51	0.27
OJPgw24	68.75	0.54	16.05	2.44	0.03	1.37	4.40	4.83	1.40	0.19	100	119.21	1.52	0.55	12.25	0.87	18.84	42.70	635.46	5.21	19.72	75.38	2315.14	0.48	0.14	0.47	2.97	0.09	0.28	0.02
OJPgw9	68.69	0.25	16.23	2.29	0.06	1.27	4.93	4.46	1.49	0.32	100	163.40	1.50	0.58	7.15	0.97	27.00	56.25	749.51	7.14	25.26	147.39	1518.29	3.53	0.36	1.02	9.95	0.74	0.64	0.28
OJPgw5	70.69	0.14	15.82	1.41	0.06	1.15	4.35	4.93	1.45		100																									
OJPgw6	70.06	0.18	15.41	1.70	0.07	1.44	5.35	4.43	1.36		100																									
OJPgw8	68.21	0.48	16.72	2.40	0.03	1.25	4.83	4.77	1.31		100																									
OJPgw10	66.01	0.53	16.20	3.50	0.04	2.30	5.34	4.64	1.29	0.15	100																									

Table 4 – The first half of the Table is a mass balance mixture of the OJP-derived experimental tonalites with the theoretical slab-fluid in Table 3. The mixing proportion is 96% tonalite and 4% slab-fluid (same as Hastie et al. 2016a) and the scenario represents the mixing of the two components on, or close to, a slab shear surface before any volatile loss. The second half of the Table represents the composition of the tonalite + slab-fluid mixtures after they have ascended and degassed (lost their water) in the overlying crust.

Highlights

1. The first stable and preserved continental crust was derived from metabasic source regions that formed by subduction processes.
2. Preferentially, residual rutile and a slab-fluid are required in the petrogenesis of the first continents.
3. Proto-plate tectonics began in the Hadean and evolved though out geological time to become the current plate tectonic system.

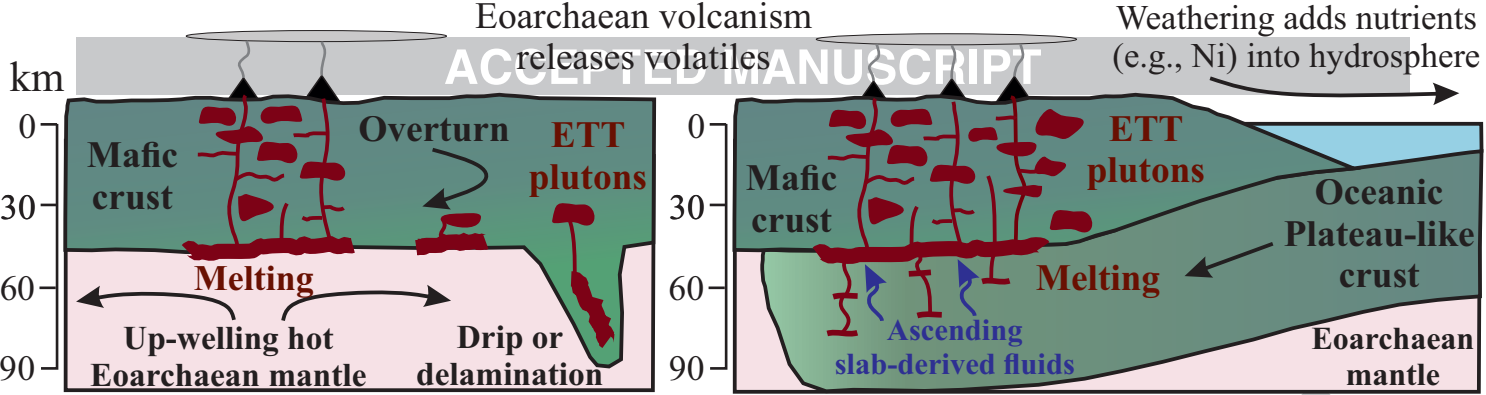

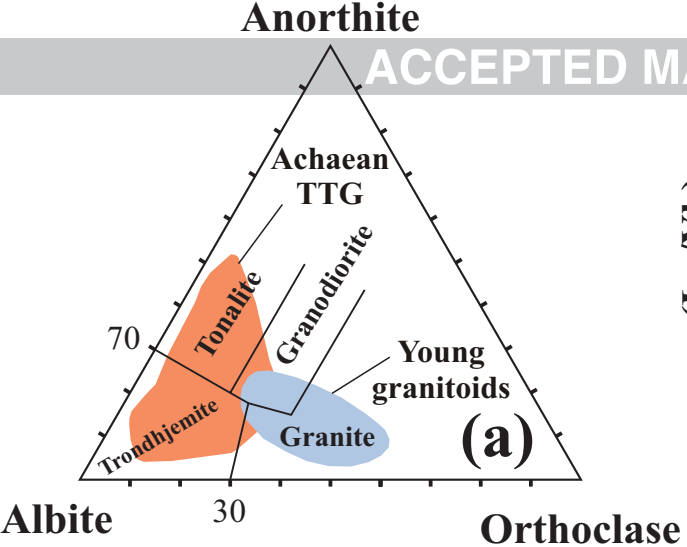

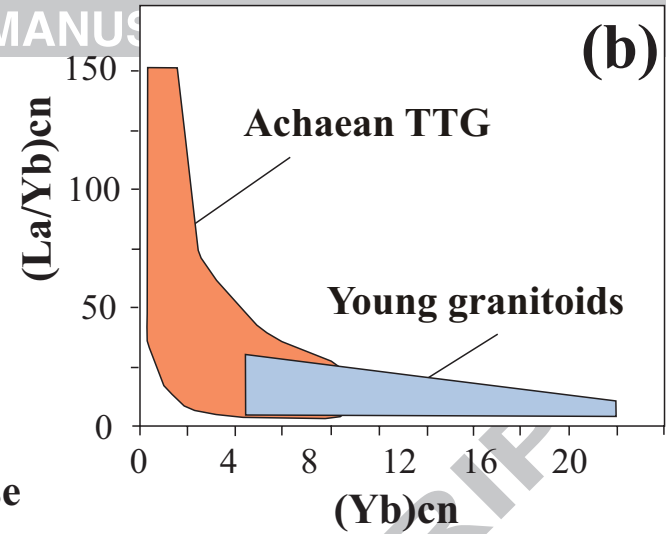

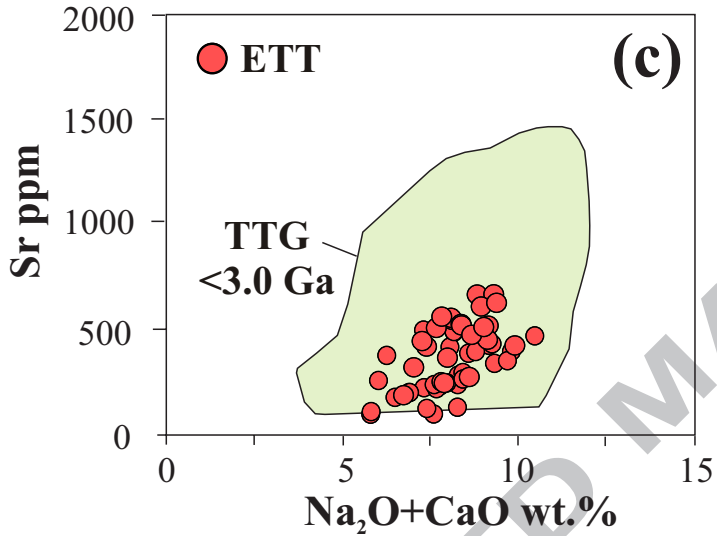

Analyses of experimental melts from Hastie et al. (2016a)

OJPgw3 - amph+plag
OJPgw11 - amph+plag
OJPgw13 - amph+plag+gnt
OJPgw9 - amph+gnt
OJPgwe1 - amph+gnt
OJPgw24 - amph+gnt

(a)

Modelled tonalite and slab fluid mixtures from Hastie et al. (2016a)

ETT

(b)

Theorectical composition of experimental melts from Hastie et al. (2016a) based on mass balance calculations

(c)

Rock/N-MORB

100
10
1
0.1
0.01

K Ba Th U Nb Ta La Ce Sr Nd Zr Ti Gd Tb Dy Ho Y Yb Lu